

# Kernel MMD Two-Sample Tests for Manifold Data

Xiuyuan Cheng\*

Yao Xie†

## Abstract

We present a study of kernel MMD two-sample test statistics in the manifold setting, assuming the high-dimensional observations are close to a low-dimensional manifold. We characterize the property of the test (level and power) in relation to the kernel bandwidth, the number of samples, and the intrinsic dimensionality of the manifold. Specifically, we show that when data densities are supported on a  $d$ -dimensional sub-manifold  $\mathcal{M}$  embedded in an  $m$ -dimensional space, the kernel MMD two-sample test for data sampled from a pair of distributions  $(p, q)$  that are Hölder with order  $\beta$  is consistent and powerful when the number of samples  $n$  is greater than  $\delta_2(p, q)^{-2-d/\beta}$  up to certain constant, where  $\delta_2$  is the squared  $\ell_2$ -divergence between two distributions on manifold. Moreover, to achieve testing consistency under this scaling of  $n$ , our theory suggests that the kernel bandwidth  $\gamma$  scales with  $n^{-1/(d+2\beta)}$ . These results indicate that the kernel MMD two-sample test does not have a curse-of-dimensionality when the data lie on the low-dimensional manifold. We demonstrate the validity of our theory and the property of the MMD test for manifold data using several numerical experiments.

## 1 Introduction

Two-sample testing, aiming to determine whether two collections of samples are from the same distribution, is one of the fundamental problems in statistics and signal processing with a wide range of applications in scientific discovery and machine learning areas. Some examples include DNA sequence signal detection [49], anomaly detection [7, 8, 3], change-point detection [47, 6, 46], and model criticism [29, 11, 4], general data analysis of biomedical data, audio and imaging data, [5, 12, 25, 9], as well as machine learning applications [28, 30, 42, 11, 26, 31].

Traditional statistical methods for two-sample tests have been focusing on the parametric or low-dimensional testing scenario, such as Hotelling’s two-sample test [23] and Student’s t-test [33]. When it is difficult to specify the exact parametric form of the distributions, non-parametric two-sample tests are more appropriate. Earlier works for non-parametric two-sample tests based on the Kolmogorov-Smirnov distance [34, 27], the total variation distance [19]. Modern Non-parametric tests for high-dimensional data have been developed and many are based on the

---

\*Department of Mathematics, Duke University. Email: xiuyuan.cheng@duke.edu

†H. Milton Stewart School of Industrial and Systems Engineering, Georgia Institute of Technology. Email: yao.xie@isye.gatech.edu. The work of Yao Xie is partially supported by an NSF CAREER Award CCF-1650913, DMS-1938106, DMS-1830210, and CMMI-1917624.

integral probability metrics [41]. A notable contribution includes the kernel Maximum Mean Discrepancy (MMD) two-sample test [15, 17, 18], which is related to U-statistics [38]. More recently, Wasserstein distance two-sample test has also been considered [14, 35]. However, it is well-known that non-parametric two-sample tests face difficulties for high-dimensional data, since the sample complexity for estimating those distance functions suffer from the curse of dimensionality. For instance, as pointed out in [37], the power of MMD-based tests decreases polynomially with an increasing dimension of target distributions.

The manifold data assumption naturally arises in applications such as imaging, video, and computer vision data. Such high-dimensional data has an intrinsic low-dimensional structure, which can be leveraged to bring performance gain in many settings. In the geometrical data analysis and manifold learning literature, seminal works [1, 2, 20, 13] show that the graph diffusion process on a kernelized affinity graph constructed using high-dimensional data vectors converges to a continuous diffusion process on the manifold, as the sample size increases to infinity and the kernel bandwidth decrease to zero. [40] and follow-up works show the approximation error to the manifold diffusion operator at a finite sample size, where the sampling complexity only involves the intrinsic dimensionality of the underlying data manifold. In the context of kernel density estimation (KDE), [32] shows that for data distribution lying on a submanifold embedded in the high-dimensional space, the convergence rate of the kernel density estimation only depends on the intrinsic dimensionality of the submanifold.

In the kernel MMD literature, the role of the kernel bandwidth and the data dimensionality was not explicitly specified in the original kernel MMD paper [16]. For kernel MMD in the high dimension setting, [36] provided a negative result that test power decreases when applying to detect mean shift of high-dimensional Gaussian distributions as the dimension increases. However, it is unclear whether the similar effect – decreasing test power for an increasing data dimension – will exhibit for manifold data, particularly when the data have intrinsically low-dimensional structure. It is also unclear how to choose the kernel bandwidth for manifold data, which usually has a significant impact on the performance of kernel-based methods.

## 1.1 Main results

This paper provides a positive answer for the question above regarding kernel MMD tests applied to high-dimensional data lying on a low-dimensional manifold. Theoretically, we show that when data densities are supported on a  $d$ -dimensional sub-manifold  $\mathcal{M}$  embedded in an  $m$ -dimensional space, the kernel MMD two-sample test is consistent and powerful when the number of samples  $n$  is greater than  $\delta_2(p, q)^{-2-d/\beta}$  up to a certain constant, and to achieve testing consistency under this scaling of  $n$ , the kernel bandwidth  $\gamma$  scales with  $n^{-1/(d+2\beta)}$ . The result holds for distributions  $p$  and  $q$  in the Höder class  $\mathcal{H}^\beta(\mathcal{M})$ ,  $0 < \beta \leq 2$ , and the squared  $\ell_2$  divergence  $\delta_2(p, q)$  is defined to be  $\int_{\mathcal{M}} (p(x) - q(x))^2 dV(x)$ . We characterize the finite-sample level and the power of the kernel MMD two-sample test, and show that the properties are only affected by the intrinsic dimensionality  $d$  of the manifold data, rather than the ambient dimensionality  $m$ .

We first prove the MMD test consistency result when data densities lie on a smooth manifold without boundary and then extended to submanifolds with a smooth boundary for Hölder class

**Table 1:** List of default notations

|                         |   |                      |   |
|-------------------------|---|----------------------|---|
| $m$                     | dimensionality of ambient space                                   | $L_\rho$             | Upper bound of Hölder constants of $p$ and $q$ on $\mathcal{M}$                                 |
| $d$                     | intrinsic dimensionality of the manifold                          | $\rho_{\max}$        | Uniform upper bound of $p$ and $q$ on $\mathcal{M}$   |
| $\mathcal{M}$           | $d$ -dimensional manifold in $\mathbb{R}^m$                       | $\gamma$             | kernel bandwidth parameter  |
| $dV$                    | volume form on $\mathcal{M}$                                      | $K_\gamma$           | kernel function $K_\gamma(x, y) = h(\frac{\ x-y\ ^2}{\gamma^2})$                                |
| $d_{\mathcal{M}}(x, y)$ | manifold geodesic distance  | $h$                  | a $C^1$ and decay function on $[0, \infty)$ , $h \geq 0$  |
| $\ x-y\ $               | Euclidean distance in $\mathbb{R}^m$                              | $m_0$                | $m_0[h] := \int_{\mathbb{R}^d} h( u ^2) du$   |
| $p, q$                  | data sampling densities on $\mathcal{M}$                          | Asymptotic Notations |   |
| $n_X, n_Y$              | number of samples in two-sample datasets $X$ and $Y$ respectively | $O(\cdot)$           | $f = O(g)$ : there exists $C > 0$ such that when $ g $ is sufficiently small, $ f  \leq C g $ . |
| $n, \rho_X$             | $n = n_X + n_Y$ , $n_X/n \rightarrow \rho_X$                      | $O_x(\cdot)$         | declaring the constant dependence on $x$ .  |
| $\beta$                 | Hölder class $\mathcal{H}^\beta(\mathcal{M})$                     |                      |   |

densities with  $0 < \beta \leq 1$ . When  $\beta > 1$ , there is no more improvement in the rate due to the degenerate kernel integral at the manifold boundary. The manifold with boundary setting contains, as a special case, when  $p$  and  $q$  are supported on a compact domain in  $\mathbb{R}^m$  (with smooth boundary), and then  $d = m$ . In this case, the testing consistency result still holds, but there is a curse of dimensionality for large  $m$ .

The theory also extends when the manifold data are corrupted by additive Gaussian noise in the ambient space  $\mathbb{R}^m$ . Under this model, data vectors  $x_i$  can be decomposed as  $x_i^{(c)} + \xi_i$ , where  $x_i^{(c)} \sim p_{\mathcal{M}}$  for some density  $p_{\mathcal{M}}$  supported on the manifold,  $\xi_i \sim \mathcal{N}(0, \sigma^2 I_m)$  and  $\xi_i$  is independent from  $x_i^{(c)}$ . We theoretically show that as long as the coordinate wise Gaussian noise level  $\sigma$  is less than  $\gamma/\sqrt{m}$  up to an absolute constant, the MMD kernel tests computed from noisy data  $x_i$  have the same theoretical consistency rate as from the clean data  $x_i^{(c)}$  which lie on the manifold. Thus, the test consistency is determined by the two densities  $p_{\mathcal{M}}$  and  $q_{\mathcal{M}}$  of the clean manifold data only.

We also showed using numerical experiments, that the test power can be maintained (for fixed test level) as the ambient dimensionality  $m$  increases for low-dimensional manifold data embedded in the high-dimensional space, which consist of group transformed images with increasingly refined resolution (that is, increasing image size). We also conduct experiments on noise corrupted data, where, under the theoretical regime of small additive noise, the performance of kernel MMD test on noisy data are similar to that on the clean data, as predicted by the theory. Finally, we apply kernel MMD tests to the more complicated hand-written digits dataset, which no longer lie on any known manifolds. For these high-dimensional data, experiments show that kernel bandwidth much smaller than the median distance bandwidth can give better performance.

## 1.2 Notation

A list of default notations is summarized in Table 1, and are also declared in the text. We clarify the big-O notation used in the paper: Our main result holds for large enough sample size  $n$  and small enough kernel bandwidth  $\gamma$  and does not require  $n \rightarrow \infty$ . For convenience, we use big-O notations in some lemmas and proof. Specifically,  $f = O(|g|)$  means that there is constant  $C$

such that when  $|g|$  is smaller than a threshold ( $g$  not necessarily converge to zero),  $|f| \leq C|g|$ . We may declare the needed smallness threshold of  $|g|$ , and when the condition is satisfied, the  $O(|g|)$  term has absolute value bounded by  $C|g|$ . We subscript “x” in  $O_x(\cdot)$  to denote that the constant  $C$  in big-O depends on object x. In this work, we treat constants which depend on manifold  $\mathcal{M}$  and kernel function  $h$  as absolute ones, and mainly track the constant dependence on data densities  $p$  and  $q$ . We clarify constant dependence in the text.

## 2 Preliminary

Consider the classical two-sample setting. Given two independent sets of data in  $\mathbb{R}^m$ ,

$$x_i \sim p, i.i.d., i = 1, \dots, n_X, \quad y_j \sim q, i.i.d., j = 1, \dots, n_Y, \quad (1)$$

and we assume that the data distributions follow densities  $p$  and  $q$ , respectively. In the manifold setting, we assume  $p$  and  $q$  are supported on a low-dimensional manifold embedded in  $\mathbb{R}^m$ . We call  $\mathbb{R}^m$  the ambient space. Defining  $n := n_X + n_Y$ , our results holds for sufficient large finite  $n$ . Also, we assume  $n_X$  and  $n_Y$  are proportional, that is, as  $n$  increases,  $n_X/n$  approaches  $\rho_X \in (0, 1)$ . Without loss of generality, we assume that the following *balance-ness condition* holds for all  $n$ ,

$$0.9\rho_X \leq \frac{n_X - 1}{n}, \quad 0.9(1 - \rho_X) \leq \frac{n_Y - 1}{n}, \quad 0 < \rho_X < 1. \quad (2)$$

### 2.1 Kerel MMD statistic

The (biased) empirical estimate for the squared kernel MMD statistic [16] is defined as

$$\hat{T} := \frac{1}{n_X^2} \sum_{i,i'=1} K_\gamma(x_i, x_{i'}) + \frac{1}{n_Y^2} \sum_{j,j'=1} K_\gamma(y_j, y_{j'}) - \frac{2}{n_X n_Y} \sum_{i,j} K_\gamma(x_i, y_j), \quad (3)$$

where  $K_\gamma(x, y)$  is a positive semi-definite (PSD) kernel with a user-specified *bandwidth* parameter  $\gamma > 0$ . In this work, we consider a kernel with a fixed bandwidth, that is,

$$K_\gamma(x, y) = h\left(\frac{\|x - y\|^2}{\gamma^2}\right), \quad h : [0, \infty) \rightarrow \mathbb{R}, \quad (4)$$

where  $h$  usually is some non-negative function. A prototypical case is the Gaussian RBF kernel with  $h(z) = \exp(-z/2)$ . Classical theory of kernel MMD test requires the kernel to be characteristic so that the MMD distance is a metric of distributions [16]. In this work, we assume that  $h$  is a non-negative,  $C^1$  and decaying function, and  $h(0) = 1$ ; see Assumption 3.3 later.

The unbiased estimator of the kernel MMD removes the diagonal entries  $K(x_i, x_i)$  and  $K(y_j, y_j)$  in the summation in (3), and has a slightly different normalization (by  $1/(N(N-1))$  rather than  $1/N^2$ , where  $N = n_X$  and  $n_Y$  respectively). Since diagonal entries always equal  $h(0)$ , which is a constant, the biased and unbiased estimators give qualitatively the same behavior in our setting. In this paper, we focus on the biased estimator (3), and the analysis can be extend

to the unbiased estimator.

## 2.2 Test level and testing power

Our concepts of the test level  $\alpha_{\text{level}}$  and the testing power follow the standard statistical definitions [16]. For the two-sample test setting, one computes the kernel MMD test statistic  $\hat{T}$  from datasets  $X$  and  $Y$ , and choose a threshold  $t_{\text{thres}}$ . The test rejects the null  $H_0$  when  $\hat{T} > t_{\text{thres}}$ .

We denote the “level” of a test as  $\alpha_{\text{level}}$ , which is also the target Type-I error. A test achieves a “level”  $\alpha_{\text{level}}$  if

$$\mathbb{P}[\hat{T} > t_{\text{thres}} | H_0] \leq \alpha_{\text{level}}, \quad (5)$$

and here,  $0 < \alpha_{\text{level}} < 1$  is typically set to a small constant; e.g.,  $\alpha_{\text{level}} = 0.05$ . To control the Type-I error (5), the threshold  $t_{\text{thres}}$  needs to be greater than the  $(1 - \alpha)$ -quantile of the distribution of  $\hat{T}$  under  $H_0$ . In theory,  $t_{\text{thres}}$  can be determined by the limiting distribution of the detection statistic  $\hat{T}$  under  $H_0$ , which is typically  $\chi^2$  in many scenarios. In practice, it is usually estimated by a standard boot-strap procedure [16, 21].

The Type-II error of the statistic  $\hat{T}$  and the threshold  $t_{\text{thres}}$  is given by  $\mathbb{P}[\hat{T} \leq t_{\text{thres}}]$  under  $H_1$ . And the *testing power* (at level  $\alpha_{\text{level}}$ ) corresponds to one minus Type-II error. Given  $\hat{T}$  and  $t_{\text{thres}}$  such that (5) holds, the testing power (with respect to alternative  $q$ ) is defined as

$$\pi(p, q; \hat{T}, t_{\text{thres}}) = \mathbb{P}[\hat{T} > t_{\text{thres}} | H_1 \text{ with } q]. \quad (6)$$

We call the test *asymptotically consistent*, if the testing power can approach 1 as samples  $n$  increases. In the following, we will characterize the testing power of kernel MMD test for a finite sample  $n$ .

## 3 Kernel MMD for manifold data

In this section, we first set up the problem for kernel two-sample test for manifold data, introduce the local kernel, and present the main result about the test size and power.

### 3.1 Manifold data in high-dimensional space

We introduce some assumptions on the manifold data and sampling densities, and start from compact manifold without boundary for simplicity:

**Assumption 3.1** (Manifold assumption).  *$\mathcal{M}$  is a  $d$ -dimensional compact  $C^\infty$  manifold isometrically embedded in  $\mathbb{R}^m$  without boundary.*

The theory extends when manifold has smooth boundary by adopting similar analysis techniques, which will be discussed in Section 4.1. Let  $\iota : \mathcal{M} \rightarrow \mathbb{R}^m$  be the isometric embedding, which is a  $C^\infty$  mapping. We use the same notation  $x$  to stand for a point  $x \in \mathcal{M}$  and  $\iota(x) \in \mathbb{R}^m$  when there is no danger of confusion. The ambient space  $\mathbb{R}^m$  has a dimensionality  $m$  possibly much larger than the intrinsic manifold dimensionality  $d$ . We denote by  $d_{\mathcal{M}}(x, y)$  the geodesic

distance on  $\mathcal{M}$ , and use  $\|x - y\|$  for the Euclidean distance in  $\mathbb{R}^m$ . Let  $dV$  be the volume form on  $\mathcal{M}$ : when  $\mathcal{M}$  is orientable,  $dV$  is the Riemann volume form; otherwise,  $dV$  is the measure associated with the local volume form. In both cases, we have  $(\mathcal{M}, dV)$  as a measure space.

In this section, we assume that data densities  $p$  and  $q$  are supported on  $\mathcal{M}$ . Extension to when data lie near to the manifold will be discussed in Section 4.2, where our analysis covers the case of additive Gaussian noise as long as the noise level is below certain threshold determined by the kernel bandwidth. Start from the case where the densities  $p$  and  $q$  are on the manifold, we assume that they are in the Hölder class  $\mathcal{H}^\beta(\mathcal{M})$ ,  $0 < \beta \leq 2$ , which means that

(i) When  $\beta \leq 1$ ,

$$\mathcal{H}^\beta(\mathcal{M}) = \{f \in C^0(\mathcal{M}), \exists L > 0, |f(x) - f(y)| \leq L d_{\mathcal{M}}(x, y)^\beta, \forall x, y \in \mathcal{M}\}, \quad (7)$$

and we define the *Hölder constant* of  $f$  as  $L_f := \sup_{x, y \in \mathcal{M}} |f(x) - f(y)| / d_{\mathcal{M}}(x, y)^\beta$ .

(ii) When  $1 < \beta \leq 2$ ,

$$\mathcal{H}^\beta(\mathcal{M}) = \{f \in C^1(\mathcal{M}), \exists L > 0, \|\nabla_{\mathcal{M}} f(x) - \nabla_{\mathcal{M}} f(y)\| \leq L d_{\mathcal{M}}(x, y)^{\beta-1}, \forall x, y \in \mathcal{M}\}, \quad (8)$$

and we define  $L_f := \|\nabla_{\mathcal{M}} f\|_\infty + \sup_{x, y \in \mathcal{M}} \|\nabla_{\mathcal{M}} f(x) - \nabla_{\mathcal{M}} f(y)\| / d_{\mathcal{M}}(x, y)^{\beta-1}$ .

Our notion of the Hölder constant  $L_f$  removes the  $C^0$  norm  $\|f\|_\infty$  from the usual definition of the Hölder norm. When  $\beta = 1$ ,  $L_f$  is the Lipschitz constant of  $f$  (with respect to manifold distance).

**Assumption 3.2** (Data density assumption). *Data densities  $p$  and  $q$  are in  $\mathcal{H}^\beta(\mathcal{M})$ ,  $0 < \beta \leq 2$ , and the Hölder constants of  $p$  and  $q$  are bounded by  $L_\rho$ . Since Hölder continuity implies continuity, due to compactness of  $\mathcal{M}$ , both densities are uniformly bounded, that is, there is constant  $\rho_{\max}$  such that*

$$0 \leq p(x), q(x) \leq \rho_{\max}, \quad \forall x \in \mathcal{M}.$$

To illustrate that the manifold structure naturally arises in real data, we give an example of high-dimensional data which lie on intrinsically low-dimensional manifolds. In addition, in this example the change of data densities  $q$  from  $p$  are induced by the change of densities on a latent manifold independent of the ambient space  $\mathbb{R}^m$ .

*Example 1* (Manifold data with increasing  $m$ ). Let data samples be images  $I_i$  which have  $W \times W$  pixels, and thus vectors in  $\mathbb{R}^m$ ,  $m = W^2$ . The image  $I_i$  is produced by evaluating a continuous function on an image grid, that is,

$$I_i(j_1, j_2) = F\left(\left(\frac{j_1}{W}, \frac{j_2}{W}\right); z_i\right), \quad 1 \leq j_1, j_2 \leq W,$$

where  $F(u; z_i)$  is a smooth mapping from  $u \in [0, 1] \times [0, 1]$  to  $\mathbb{R}$  and is parametrized by a latent variable  $z_i \in \mathcal{M}_z$ . For example, let  $\mathcal{M}_z$  be a rotation group  $SO(2)$ , and the mapping  $F(\cdot; z)$  corresponds to applying rotation action  $z \in SO(2)$  to the image, as illustrated in Figure 1.

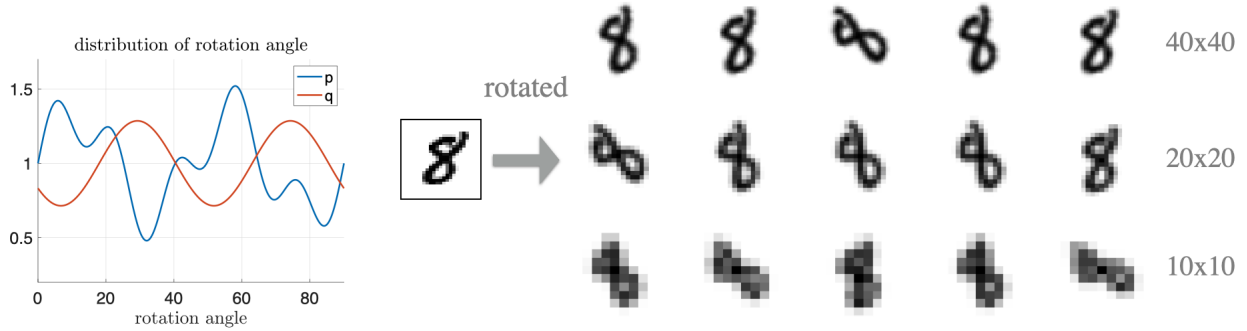


**Figure 1:** One digit image rotated by angles  $z$  from 0 to 90 degrees, and at different image sizes. The images for  $z \in [0, \frac{\pi}{2}]$  lie on a 1D manifold in the ambient space, and approaches the continuous limit as image resolution refines. The group element  $z$  have two distributions, which induce two distributions of data images in ambient space  $\mathbb{R}^m$ . The two-sample test results are provided in Section 5.

Suppose  $\mathcal{M}_z$  is  $d$ -dimensional, then, under generic assumptions on  $F$ , the continuous functions  $F(\cdot; z)$  for all  $z$  lies on a  $d$ -dimensional manifold in the function space, and when the discretization is fine enough, the images  $I_i$  lie on a manifold in  $\mathbb{R}^{W \times W}$  which approaches the manifold of continuous functions in the limit of  $W \rightarrow \infty$ . When the two distributions  $p$  and  $q$  of images  $I_i$  on the image manifold are induced by densities  $p_z$  and  $q_z$  which are distributions of  $z_i$  on  $\mathcal{M}_z$ , the latter does not change with  $W$ . Consequently, as dimensionality  $m$  increases, the  $KL(p||q)$  approaches  $KL(p_z||q_z)$  which is an  $O(1)$  limit.

### 3.2 Local kernels on manifold

Same as in the setting of traditional manifold learning analysis [13, 2, 44], we consider local kernel  $K_\gamma(x, y)$  defined as in (4), which means that the bandwidth parameter  $\gamma$  decreases as number of data samples  $n$  increases. The following class of non-negative differential kernel function  $h$  contains Gaussian RBF kernel as a special case.

**Assumption 3.3** (Differentiable kernel). *We made the following assumptions about the function  $h$ :* (C1) *Regularity.  $h$  is continuous on  $[0, \infty)$ ,  $C^1$  on  $(0, \infty)$ .*

(C2) *Decay condition.  $h$  and  $h'$  are bounded on  $(0, \infty)$  and have sub-exponential tail, specifically,  $\exists a, a_k > 0$ , s.t.,  $|h^{(k)}(\xi)| \leq a_k e^{-a\xi}$  for all  $\xi > 0$ ,  $k = 0, 1$ .*

(C3) *Non-negativity.  $h \geq 0$  on  $[0, \infty)$ . Here we assume  $h(0) = 1$ , due to the positivity of  $K(x, x) = h(0) > 0$ , and that multiplying a constant introduces a global constant normalization. By that kernel is PSD,  $|K_\gamma(x, y)| \leq h(0)$  for all  $x, y$ , thus  $a_0 = 1$ .*

Similar conditions on  $h$  have been used in [13] for kernelized graph Laplacian constructed from manifold data. For  $h$  that satisfies Assumption 3.3, we introduce the following moment constant of the kernel  $h$ ,

$$m_0[h] := \int_{\mathbb{R}^d} h(\|u\|^2) du,$$

which is finite due to (C2). By (C3) and  $h(0) = 1$ ,  $m_0[h] > 0$ .

The following lemma establishes the integral of Hölder function with local kernel on manifold.

**Lemma 3.1.** *Suppose  $\mathcal{M}$  satisfies Assumption 3.1,  $h$  satisfies Assumption 3.3, and  $f$  is in  $\mathcal{H}^\beta(\mathcal{M})$ ,  $0 < \beta \leq 2$ , with Hölder constant  $L_f$ . Then there is  $\gamma_0 > 0$  which depends on  $\mathcal{M}$  only, and constant  $C_1$  that depends on  $(\mathcal{M}, h)$ , such that when  $0 < \gamma < \min\{1, \gamma_0\}$ ,*

$$\left| \gamma^{-d} \int_{\mathcal{M}} h\left(\frac{\|x-y\|^2}{\gamma^2}\right) f(y) dV(y) - m_0[h]f(x) \right| \leq C_1(L_f \gamma^\beta + \|f\|_\infty \gamma^2), \quad \forall x \in \mathcal{M}. \quad (9)$$

*Specifically,  $\gamma_0$  depends on manifold reach and curvature, and  $C_1 > 0$  depends on manifold curvature and volume, the sub-exponential decay constant  $a$  of  $h$ , and the intrinsic dimensionality  $d$ .*

When  $L_f > 0$ , since  $\beta \leq 2$ , the  $O(\gamma^\beta)$  term will be the leading term in the r.h.s of (9). When  $\beta = 2$ , the residual term in (9) becomes  $O(\gamma^2)$ , which echos the  $O(\gamma^2)$  error term in Lemma 8 of [13], and the latter was proved for  $f$  with higher order regularity and under different technical assumptions. The proof follows the approach in [13] using standard technique of differential geometry, and is included in Section 7 for completeness.

We define

$$\begin{aligned} T &= \mathbb{E}_{x \sim p, y \sim p} K_\gamma(x, y) + \mathbb{E}_{x \sim q, y \sim q} K_\gamma(x, y) - 2\mathbb{E}_{x \sim p, y \sim q} K_\gamma(x, y) \\ &= \int_{\mathcal{M}} \int_{\mathcal{M}} K_\gamma(x, y) (p - q)(x)(p - q)(y) dV(x) dV(y), \end{aligned} \quad (10)$$

which is the population (squared) kernel MMD. We apply Lemma 3.1 to when  $f = p$  or  $q$  to obtain the following lemma, which is proved in Section 7.

**Lemma 3.2.** *Under Assumption 3.1, 3.2, 3.3,  $\gamma_0$  and  $C_1$  as in Lemma 3.1, then when  $0 < \gamma < \min\{1, \gamma_0\}$ ,*

$$T = \gamma^d \left( m_0[h] \int_{\mathcal{M}} (p(x) - q(x))^2 dV(x) + r_T \right), \quad |r_T| \leq 4C_1(L_\rho \gamma^\beta + \rho_{\max} \gamma^2). \quad (11)$$

### 3.3 Control of deviation of $\hat{T}$ from mean

We now control the deviation  $\hat{T}$  around certain expected value (with bias) using concentration of U-statistics. The U-statistic argument was used in [16] but only using the point-wise boundedness of the kernel. To obtain better concentration, we apply the Bernstein-type argument which allows to reveal the role of the bandwidth. The proof adopts the classical decoupling technique of the U-statistics [22], and is included in Section 7 for completeness.

**Proposition 3.4.** *Under Assumption 3.1, 3.2, 3.3, and the balanceness condition (2). Define*

$$c := 0.9 \min\{\rho_X, 1 - \rho_X\}, \quad \nu := (m_0[h^2] + 1)\rho_{\max}. \quad (12)$$



Then, there is a constant  $C_1^{(2)} > 0$  which depends  $(\mathcal{M}, h)$ , s.t. when  $0 < \gamma < \min\{1, \gamma_0, (C_1^{(2)})^{-1/2}\}$ ,  
(1) Under  $H_0$ , for  $0 < \lambda < 3\sqrt{c\nu\gamma^d n}$ , w.p.  $\geq 1 - 3e^{-\lambda^2/8}$ ,

$$\hat{T} \leq \frac{4}{cn} + 4\lambda\sqrt{\frac{\nu}{c} \frac{\gamma^d}{n}},$$

(2) Under  $H_1$ , let  $T$  be defined as in (10), for  $0 < \lambda < 3\sqrt{c\nu\gamma^d n}$ , w.p.  $\geq 1 - 3e^{-\lambda^2/8}$ ,

$$\hat{T} \geq T - 4\lambda\sqrt{\frac{\nu}{c} \frac{\gamma^d}{n}}.$$

The constant  $C_1^{(2)}$  corresponds to the constant  $C_1$  in Lemma 3.1 with  $h$  replaced by  $h^2$ .

The proof of Proposition 3.4 is left to Section 7. Because that analysis uses U-statistic argument, it obtains  $O(n^{-1/2})$  fluctuation of the statistics  $\hat{T}$  around the mean (up to the  $O(n^{-1})$  bias) under both  $H_0$  and  $H_1$ . Note that, under  $H_0$ , the deviation can be expected to scale as  $O(n^{-1})$  [16, 9]. While this could make a difference in terms of choosing test threshold  $t$  (if one uses the limiting density), it does not affect our proof of the testing power in Theorem 3.5, because the deviation of  $\hat{T}$  under  $H_1$  is of order  $O(n^{-1/2})$  will be the dominating term over the deviation of  $\hat{T}$  under  $H_0$ . In practice, the testing threshold is usually estimated empirically by boot-strap methods rather than chosen according to theory, see more in Section 5. We thus postpone the improvement of the concentration of  $\hat{T}$  under  $H_0$  in the current work.

### 3.4 MMD test size and power

We are ready to derive the main theorem on kernel MMD test's size and power at finite sample size:

**Theorem 3.5** (Size and power of kernel MMD test on manifold). *Under Assumptions 3.1, 3.2, 3.3, and the balanceness condition (2), let the constants  $c$ ,  $\nu$ , and  $C_1^{(2)}$  be as in Proposition 3.4, and  $\gamma_0$  and  $C_1$  as in Lemma 3.1. Define*

$$\lambda_1 = \sqrt{8 \log(3/\alpha_{\text{level}})},$$

and let the threshold for the test be

$$t_{\text{thres}} = \frac{4}{cn} + 4\lambda_1\sqrt{\frac{\nu}{c} \cdot \frac{\gamma^d}{n}}.$$

For  $q \neq p$  under  $H_1$ , define

$$D_{p,q} := m_0[h] \int_{\mathcal{M}} (p(x) - q(x))^2 dV(x) > 0.$$

Then, when  $\gamma$  is small enough such that

$$0 < \gamma < \min \left\{ 1, \gamma_0, (C_1^{(2)})^{-1/2} \right\}, \quad L_\rho \gamma^\beta + \rho_{\max} \gamma^2 < \frac{0.1 D_{p,q}}{4C_1}, \quad (13)$$

and meanwhile, for some constant  $\lambda_2 > 0$ ,  $n$  is large enough such that

$$\gamma^d n > \max \left\{ \frac{1}{c\nu} \left( \frac{\max\{\lambda_1, \lambda_2\}}{3} \right)^2, \frac{10}{cD_{p,q}}, \frac{\nu}{c} \left( \frac{8(\lambda_1 + \lambda_2)}{D_{p,q}} \right)^2 \right\}, \quad (14)$$

then

$$\begin{aligned} \mathbb{P}[\widehat{T} > t_{\text{thres}} | H_0] &\leq \alpha_{\text{level}}, \\ \mathbb{P}[\widehat{T} \leq t_{\text{thres}} | H_1] &\leq e^{-\lambda_2^2/8}. \end{aligned} \quad (15)$$

Since the constants  $m_0[h^2]$  appears in  $\nu$ , and  $m_0[h]$  appears in  $D_{p,q}$ , here we derive explicit constants for Gaussian RBF kernel.

*Example 2* (Constants for Gaussian  $h$ ). When  $h(\xi) = e^{-\xi^2/2}$ ,

$$m_0[h] = \int_{\mathbb{R}^d} e^{-|u|^2/2} du = (2\pi)^{d/2}, \quad m_0[h^2] = \int_{\mathbb{R}^d} e^{-|u|^2} du = \pi^{d/2},$$

both of which are constants depending on  $d$ .

Theorem 3.5 considers a fixed alternative  $q$ , yet the bound of testing power holds for finite samples and finite  $\gamma$ , and thus the result can address certain asymptotic scenarios where  $q - p$  decreases to zero as  $n$  increases. In Theorem 3.5, only the intrinsic dimensionality  $d$  affects the testing power but not the ambient space dimensionality  $m$ . The constants  $D_{p,q}$ ,  $\rho_{\max}$ , and  $L_\rho$  are determined by  $p$  and  $q$  as Hölder functions on  $(\mathcal{M}, dV)$ , which are intrinsically defined.

*Remark 3.1* (Condition for test consistency). Under the setting of manifold densities  $p$  and  $q$ , define

$$\delta_2 := \delta_2(p, q) = \int_{\mathcal{M}} (p(x) - q(x))^2 dV(x), \quad D_{p,q} = m_0[h] \delta_2.$$

We consider where  $\delta_2$  is small such that the 3rd term in (14) achieves the maximum among the three. Here we treat  $\lambda_1$  and  $\lambda_2$  as  $O(1)$  fixed constants. Theorem 3.5 implies that the kernel MMD two-sample test is consistent and the test power approaches 1 exponentially fast as number of samples  $n$  increases if

- (i)  $\gamma$  can be chosen to be smaller than some  $O(1)$  threshold determined by  $(\mathcal{M}, h)$ , and also small enough such that, for  $c_1 > 0$  which depends on  $(L_\rho, \rho_{\max})$  and  $m_0[h]$ ,

$$\gamma^\beta < c_1 \delta_2,$$

Here we use the  $O(\gamma^\beta)$  term in the condition (13) because  $\beta \leq 2$ .

(ii)  $n$  is sufficiently large to make

$$\gamma^d n > \frac{c_2}{\delta_2^2},$$

where  $c_2 > 0$  depends on  $\rho_{\max}$ ,  $\rho_X$  and  $(\mathcal{M}, h)$ .

Putting together, it means that, for such small  $\delta_2$ , the threshold for  $n$  to give testing power is when

$$n \gtrsim \delta_2^{-2-d/\beta}, \quad \text{with } \gamma \sim n^{-1/(d+2\beta)} \quad (16)$$

up to constants which are omitted. This means that the smallest  $\delta_2(p, q)$  that can be detected by the kernel MMD test is  $\delta_2 \gtrsim n^{-1/(2+d/\beta)}$ . In particular, when  $\beta = 2$ , this becomes  $\delta_2 \gtrsim n^{-1/(2+d/2)}$ , and the choice of bandwidth  $\gamma$  is at the order of  $n^{-1/(d+4)}$ .

*Remark 3.2* (Choice of bandwidth). As shown in (16), at the critical regime of detectability by the test where  $\delta_2$  is small, the bandwidth needs to scale with  $n^{-1/(d+2\beta)}$  so that the test can have power. The scaling echos the classical theory of density estimation [45]. This choice of  $\gamma$  leads to local kernels for the manifold MMD test, where  $\gamma \rightarrow 0$  as  $n$  increases. In contrast, the median distance choice of bandwidth [16] may lead to  $\gamma$  which is of  $O(1)$ : on a manifold of diameter  $O(1)$ , suppose the data density is uniform, then the median of pairwise distance is generally  $O(1)$ . Thus the median distance  $\gamma$  may not be optimal in practice for high-dimensional data, e.g., when data lie on or near to intrinsically low-dimensional manifold or sub-manifolds and there are sufficiently many samples in the dataset to detect a small departure of the density. We compare MMD with smaller bandwidths and the median distance bandwidth in experiments in Section 5.

*Proof of Theorem 3.5.* Under the condition of the theorem, the conditions needed by Proposition 3.4 and Lemma 3.2 are both satisfied. We first verify that the Type-I error is at most  $\alpha_{\text{level}}$ . The definition of  $\lambda_1$  makes that  $3e^{-\lambda_1^2/8} = \alpha_{\text{level}}$ . By the definition of  $t_{\text{thres}}$  and Proposition 3.4(1), the type-I error bound holds as long as  $\lambda_1 < 3\sqrt{c\nu\gamma^d n}$ , and this is guaranteed by (14).

Next we address the Type-II error. By Proposition 3.4(2), the bound  $e^{-\lambda_2^2/8}$  holds as long as  $\lambda_2 < 3\sqrt{c\nu\gamma^d n}$  and

$$t_{\text{thres}} < T - 4\lambda_2 \sqrt{\frac{\nu}{c} \frac{\gamma^d}{n}}. \quad (17)$$

By Lemma 3.2,  $T = \gamma^d(D_{p,q} + r_T)$ , and  $|r_T| \leq 4C_1(L_\rho\gamma^\beta + \rho_{\max}\gamma^2)$ . By (13), we have

$$|r_T| < 0.1D_{p,q},$$

and then  $T > \gamma^d 0.9D_{p,q}$ . Meanwhile, (14) gives that

$$\frac{4}{cn} < 0.4\gamma^d D_{p,q}, \quad 4(\lambda_1 + \lambda_2) \sqrt{\frac{\nu}{c} \frac{\gamma^d}{n}} < 0.5\gamma^d D_{p,q}. \quad (18)$$

Thus,  $\frac{4}{cn} + 4(\lambda_1 + \lambda_2) \sqrt{\frac{\nu}{c} \frac{\gamma^d}{n}} < 0.9\gamma^d D_{p,q} < T$ , which implies (17) by the definition of  $t_{\text{thres}}$ .  $\square$

## 4 Extensions

### 4.1 Manifold with boundary

In this section, we show that the theoretical results in Section 3 extend when the data manifold  $\mathcal{M}$  has smooth boundary  $\partial\mathcal{M}$ , that is,

**Assumption 4.1.**  $\mathcal{M}$  is a  $d$ -dimensional compact  $C^\infty$  sub-manifold isometrically embedded in  $\mathbb{R}^m$ , where the boundary  $\partial\mathcal{M}$  is also  $C^\infty$ .

The proof uses similar techniques, and is based on the local kernel integral lemma, Lemma 4.1, which handles when  $x$  is on or near to  $\partial\mathcal{M}$ . Theorem 3.5 then extends with certain changes in the constants and condition 13, due to the degenerate approximation error terms at the manifold boundary in Lemma 4.1. See the specifics in below.

*Remark 4.1.* When data densities  $p$  and  $q$  are compactly supported on some domain  $\Omega$  in  $\mathbb{R}^m$  and  $\Omega$  has smooth boundary, this is a special case of the manifold-with-boundary setting where  $d = m$ . Our theoretical result thus covers such cases. When  $m$  is large, there is a curse of dimensionality revealed by the  $\gamma^d$  factor in the required lower bound of  $n$  in the condition (14).

We start by establishing the following lemma, which is the counter-part of Lemma 3.1 for  $0 < \beta \leq 1$ . All poofs in this subsection are left to Section 7.2

**Lemma 4.1.** Suppose  $\mathcal{M}$  satisfies Assumption 4.1,  $h$  satisfies Assumption 3.3, and  $f$  is in  $\mathcal{H}^\beta(\mathcal{M})$ ,  $0 < \beta \leq 1$ , with Hölder constant  $L_f$ . Let  $d_E(x, \partial\mathcal{M})$  denote the Euclidean distance from  $x \in \mathcal{M}$  to  $\partial\mathcal{M}$ , and define  $\delta_\gamma := \sqrt{1.2 \frac{d+10}{a} \gamma^2 \log \frac{1}{\gamma}}$ . Then, there is  $\gamma'_0 > 0$  which depends on  $\mathcal{M}$  only, and constant  $C'_1$  that depends on  $(\mathcal{M}, h)$  such that when  $0 < \gamma < \min\{\gamma'_0, 1\}$ , for any  $x$  such that  $d_E(x, \partial\mathcal{M}) \leq \delta_\gamma$ ,

$$\left| \gamma^{-d} \int_{\mathcal{M}} h\left(\frac{\|x-y\|^2}{\gamma^2}\right) f(y) dV(y) - m_0^{(\gamma)}[h](x) f(x) \right| \leq C'_1 (L_f \gamma^\beta + \|f\|_\infty \gamma^2), \quad (19)$$

where  $0 \leq m_0^{(\gamma)}[h](x) \leq m_0[h]$  for all  $x$ ; When  $d_{\text{Euc}}(x, \partial\mathcal{M}) > \delta_\gamma$ , (19) holds with  $m_0^{(\gamma)}[h](x)$  replaced with  $m_0[h]$ .

*Remark 4.2.* Similarly as in Lemma 3.1,  $\gamma'_0$  depends on manifold reach and curvature, and the constant  $C'_1$  depends on manifold curvature and volume, and the kernel function  $h$ . When  $1 < \beta \leq 2$ , previously in Lemma 3.1 the  $O(\gamma^\beta)$  term can further improve, however, when  $x$  is near or on the boundary  $\partial\mathcal{M}$ , even when  $f$  is  $C^1$ , there will be a  $O(\|\nabla_{\mathcal{M}} f\|_\infty \gamma)$  residual term due to that the integral of  $h(\|u\|^2/\gamma^2)u$  on half of  $\mathbb{R}^d$  no longer vanishes. Thus we only derive the bound for  $\beta \leq 1$  here.

We then extend Lemma 3.2 which bounds the error between  $\gamma^{-d}T$  and  $m_0[h]C_{p,q}$ :

**Lemma 4.2.** Under Assumptions 4.1, 3.2, 3.3,  $\gamma'_0$  and  $C'_1$  as in Lemma 4.1, then when  $0 < \gamma < \min\{1, \gamma'_0\}$ ,  $T = \gamma^d (m_0[h] \int_{\mathcal{M}} (p(x) - q(x))^2 dV(x) + r_T)$ , and

$$|r_T| \leq 4 \left( C'_1 (L_\rho \gamma^\beta + \rho_{\max} \gamma^2) + C'_2 \rho_{\max}^2 \gamma \sqrt{\log \frac{1}{\gamma}} \right), \quad (20)$$

where  $C'_2$  depends on manifold curvature, the regularity and volume of manifold boundary  $\partial\mathcal{M}$ ,  $d$  and  $h$ .

Finally, to extend Proposition 3.4, it suffices to bound the integral

$$\mathbb{E}_{x \sim p, y \sim p} K_\gamma(x, y)^2 \leq \nu \gamma^d, \quad (21)$$

where  $\nu$  is defined as in (12). We prove in Section 7.2 that this is the case when  $\gamma < (C_1'^{(2)})^{-1/2}$ , where  $C_1'^{(2)}$  corresponds to the constant  $C'_1$  in Lemma 4.1 replacing  $h$  with  $h^2$ , and thus  $C_1'^{(2)}$  only depends on  $(\mathcal{M}, h)$ . The upper bounds of  $\mathbb{E}_{x \sim q, y \sim q} K_\gamma(x, y)^2$  and  $\mathbb{E}_{x \sim p, y \sim q} K_\gamma(x, y)^2$  are similar. Thus the same deviation bound as in Proposition 3.4 can be proved after replacing the constants  $C_1^{(2)}$  with  $C_1'^{(2)}$ , and  $\gamma_0$  with  $\gamma'_0$ , in the statement. The main theorem Theorem 3.5 then directly follows, with the following changes: (i) replacements of the constants  $\gamma_0, C_1, C_1^{(2)}$  with those with primes, (ii) Condition (13) is replaced by

$$4 \left( C_1' (L_\rho \gamma^\beta + \rho_{\max} \gamma^2) + C_2' \rho_{\max}^2 \gamma \sqrt{\log \frac{1}{\gamma}} \right) < 0.1 D_{p,q},$$

due to the extra error term involving  $C_2'$  in Lemma 4.2.

We have extended the theory to data manifold with smooth boundary. Inline with the theoretical results, the experiments in Section 5 are conducted on manifold data where  $\mathcal{M}$  has boundary, for both the constructed manifold of image data by group action in Section 5.2, and the original MNIST data which lie close to certain collection of sub-manifolds in the ambient space in Section 5.3.

## 4.2 Near-manifold data

In applications, data points may not lie exactly on the low-dimensional manifold but only near to it. Since kernel  $K_\gamma(x, y)$  is computed from Euclidean distances among data points, one can expect that if data samples are lying within distance proportional to  $\gamma$  from the manifold  $\mathcal{M}$ , then the integration of kernel  $K_\gamma(x, y)$  over such data distributions will preserve the magnitude to be of order  $\gamma^d$  and will not have curse of dimensionality.

An important case is when near-manifold data are produced by adding Gaussian noise, which are distributed as  $\mathcal{N}(0, \sigma^2 I_m)$ , to data points which are lying on manifold. In this case, to make the off-manifold perturbation to be of length up to a constant times of  $\gamma$  (with high probability), it allows  $\sigma$  to be up to  $c\gamma/\sqrt{m}$  for some  $c > 0$ . Here, we show that Theorem 3.5 can be extended under this noise regime.

Specifically, let  $x_i = x_i^{(c)} + \xi_i^{(1)}$ ,  $x_i^{(c)} \sim p_{\mathcal{M}}$ ,  $\xi_i^{(1)} \sim \mathcal{N}(0, \sigma_{(1)}^2 I_m)$ , and  $y_i = y_i^{(c)} + \xi_i^{(2)}$ ,  $y_i^{(c)} \sim q_{\mathcal{M}}$ ,  $\xi_i^{(2)} \sim \mathcal{N}(0, \sigma_{(2)}^2 I_m)$ , where the manifold clean data  $x_i^{(c)}$  and  $y_i^{(c)}$  are independent from the ambient space Gaussian noise  $\xi_i^{(1)}$  and  $\xi_i^{(2)}$ . When  $p_{\mathcal{M}}$  and  $q_{\mathcal{M}}$  satisfies Assumption 3.2 and  $h$  is Gaussian kernel, Theorem 3.5 extends when

$$\sigma_{(1)}^2 + \sigma_{(2)}^2 \leq \frac{c^2}{m} \gamma^2,$$

for some  $c > 0$ . The argument is based on that the proof of Theorem 3.5 relies on the approximation of kernel integrals  $\mathbb{E}_{x \sim p, y \sim p} K_\gamma(x, y)$  and the boundedness of  $\mathbb{E}_{x \sim p, y \sim p} K_\gamma(x, y)^2$  at the order  $O(\gamma^d)$ , and similarly with  $\mathbb{E}_{x \sim p, y \sim q}$ ,  $\mathbb{E}_{x \sim q, y \sim q}$ . Thus, when kernel  $h$  is Gaussian, and  $p$  (and  $q$ ) equals  $p_{\mathcal{M}}$  (and  $q_{\mathcal{M}}$ ) convolved with a Gaussian with coordinate variance  $\gamma^2/m$  in  $\mathbb{R}^m$ , these integrals can be shown to be equivalent to those integrated over  $p_{\mathcal{M}}$  and  $q_{\mathcal{M}}$  with another Gaussian kernel having bandwidth  $\tilde{\gamma}$ , where  $\tilde{\gamma}/\gamma$  is bounded between 1 and the absolute constant  $\sqrt{1 + c^2/m}$ . As a result, the integrals of  $K_\gamma(x, y)$  and  $K_\gamma(x, y)^2$  can be computed same as before in Lemma 3.2 and Proposition 3.4, leading to a result of Theorem 3.5 after replacing the roles of  $p$  and  $q$  with  $p_{\mathcal{M}}$  and  $q_{\mathcal{M}}$ . Details are left to Section 7.3.

This suggests that when the coordinate-wise noise level  $\sigma$  in  $\mathbb{R}^m$  is bounded at the level of  $\gamma/\sqrt{m}$ , the behavior of the two-sample test with kernel  $K_\gamma(x, y)$  applied to manifold plus noise data is essentially close to as if applied to the clean data on the manifold, and the testing power is determined by the on-manifold distributions  $p_{\mathcal{M}}$  and  $q_{\mathcal{M}}$ . Experiments of data with additive Gaussian noise are given in Section 5.2, which verifies this theoretical prediction. In practice, with finitely many samples and dimensionality, the testing performances on clean and noisy data will stay close for small noise level  $\sigma$ , and start to have discrepancy when  $\sigma$  exceeds certain level allow by the theoretical range above.

## 5 Numerical experiments

In this section, we present several numerical examples to demonstrate the validity of our theory. We first present an algorithm for evaluating the threshold of the test, and then a synthetic example with images, and finally, a density departure example using the MNIST data.

### 5.1 Algorithm and bootstrap estimation of $t_{\text{thres}}$

We use the Gaussian RBF kernel in all the experiments and use the vanilla  $O(n^2)$  algorithm to construct the kernel matrix and compute the MMD statistic. The summary of the algorithm is as follows

*Input data:*  $X$  and  $Y$ , each having  $n_X$  and  $n_Y$  samples

*Parameters:* kernel bandwidth  $\gamma$ , test threshold  $t_{\text{thres}}$  if available.

*Step 1.* Construct the  $n$ -by- $n$  kernel matrix,  $n = n_X + n_Y$ ,

$$K = \begin{bmatrix} K_{XX}, K_{XY} \\ K_{XY}^T, K_{YY} \end{bmatrix},$$

where  $K_{XX} = (K_\gamma(x_i, x_j))_{1 \leq i, j \leq n_X}$ ,  $K_{YY} = (K_\gamma(y_i, y_j))_{1 \leq i, j \leq n_Y}$ , and  $K_{XY} = (K_\gamma(x_i, y_j))_{1 \leq i \leq n_X, 1 \leq j \leq n_Y}$ .

*Step 2.* Compute  $\hat{T}$  as defined in (3) from the kerne matrix  $K$ .

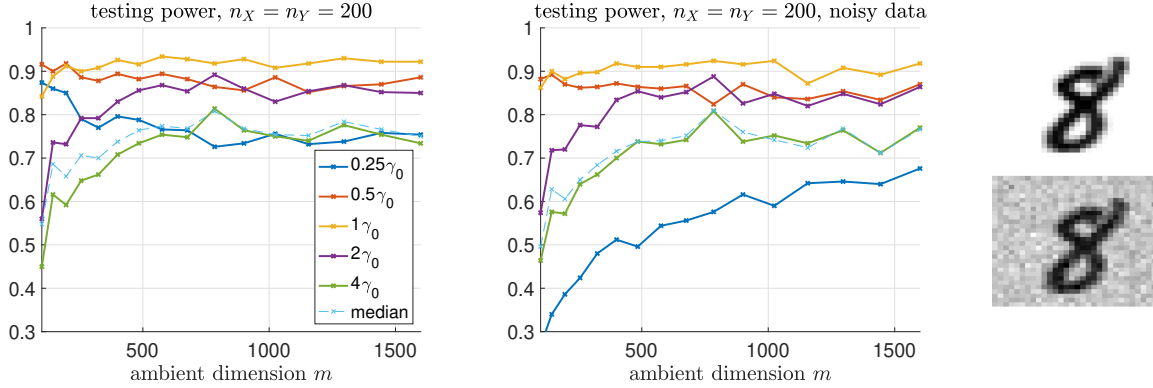


**Figure 2:** Kernel MMD on two datasets of rotated images with different distributions of rotation angles. Images are of sizes  $10 \times 10, \dots, 40 \times 40$ , and thus  $m$  increases from 100 to 1600. The test are computed with 5 values of kernel bandwidth as in (22), and that chosen by the median distance from data. The test power is estimated using  $n_{run} = 500$ . (Left) Results on clean images. (Middle) Results on images with additive Gaussian noise, where noise level is chosen to be small and satisfies the condition in Section 4.2. (Right) Example clean and noisy images (size  $30 \times 30$ ).

*Step 3.* If  $\hat{T} < t_{\text{thres}}$ , accept  $H_0 : p = q$ , otherwise, reject  $H_0$ .

If the test threshold  $t_{\text{thres}}$  is not provided, we use the bootstrap procedure (called “permutation test” in [16, 36]) to estimate it from data: Given the computed kernel matrix  $K$ , and target test level  $\alpha_{\text{level}}$ ,

*Step 4.* Repeating  $l = 1, \dots, n_{\text{boot}}$  times:

- Randomly permute the rows and columns of  $K$  simultaneously, obtain a matrix  $K_l$
- Compute the statistic  $\hat{T}_l$  from  $K_l$ , treating the first  $n_X$  rows and columns are from one dataset and the other  $n_Y$  rows and columns from another data set.

*Step 5.* From the empirical distribution of  $n_{\text{boot}}$ , evaluate the  $(1 - \alpha_{\text{level}})$ -quantile as  $t_{\text{thres}}$ .

Note that in the bootstrap procedure for threshold evaluation, no re-computing of the kernel matrix  $K$  is needed, but only the block average over the  $n^2$  entries according to the permuted two sample class labels. The testing power is estimated by  $n_{run}$  random replicas of the experiments and count the frequency that the test is corrected rejected when  $q \neq p$ . In our experiments, we use  $\alpha_{\text{level}} = 0.05$ ,  $n_{\text{boot}}$  and  $n_{run}$  a few hundreds.

In our experiments, we test over a range of kernel bandwidth parameters  $\gamma$ . In practice,  $\gamma$  can also be chosen adaptively from data, e.g., the *median distance bandwidth* is set to be the median of all pairwise distances in the two sample datasets. Our theory in Section 3 suggests that the median distance  $\gamma$  may not be the optimal choice, and on certain manifold data of intrinsically low dimensionality, when there are sufficiently many samples, kernel of smaller bandwidth can have better testing power. We compare different bandwidth choices in experiments.

## 5.2 Images with differently distributed rotation angles

### 5.2.1 Clean data

In this section, we construct two datasets consisting of randomly rotated copies of a digit image which are resized to be of different resolutions. The data generating process was introduced in Example 1 and illustrated in Figure 1. The distributions  $p$  and  $q$  of the two datasets are induced by different rotation angle distributions, and the densities of rotation angles (between 0 to 90 degrees) are shown in the left of Figure 1. The image sizes change from  $10 \times 10$  to  $40 \times 40$ , and as a result, the data dimensionality increases from 100 to 1600. Note that since the rotation is only up to  $\pi/2$ , the corresponding manifold is a 1D curve with two endpoints, namely a manifold with boundary.

Note that the image pixels values maintain the same magnitude as  $W$  increases, and then  $\frac{1}{m} \sum_{u=1}^m I_i(u)^2$  approaches an  $O(1)$  limit, which is the squared integral of the underlying continuous function on  $[0, 1]^2$ . This means that the image data vectors of size  $W \times W$  need to divide by  $\sqrt{m}$ ,  $m = W^2$ , so as to obtain isometric embedding of a manifold of diameter  $O(1)$  in  $\mathbb{R}^m$ . In experiments we use bandwidth  $\gamma$  to resized images, can we call  $\gamma/\sqrt{m}$  the “pixel-wise bandwidth”. The pixel-wise bandwidth corresponds to the “ $\gamma$ ” in the theory in Section 3.

In computing the kernel MMD, we use bandwidth parameter over 5 values such that

$$\frac{\gamma}{\sqrt{m}} = \gamma_0 \left\{ \frac{1}{4}, \frac{1}{2}, 1, 2, 4 \right\}, \quad m = W^2, \quad W = 10, \dots, 40, \quad (22)$$

with  $\gamma_0 = 20$ , which is the baseline pixel-wise bandwidth. The median distance gives the pixel-wise bandwidth about 70. Since the grayscale images take pixel values between 0 and 255, the pixel-wise bandwidth being 20 is relatively small, and is smaller than that chosen by the median distance. The estimated two-sample testing power on clean images is shown in Figure 2 (Left), which is computed using  $n_{\text{boot}} = 400$  and  $n_{\text{run}} = 500$ . It can be seen that all the bandwidth choices give certain test power, which is consistent across  $m$  after  $m$  is large enough (from 500 to 1600). The performance with pixel-wise bandwidth equals 20 appears to be the best and is better than the bandwidth by median distance.

### 5.2.2 Noisy data

We add pixel-wise Gaussian noise of standard deviation  $\sigma_0 = 20$  to the resized image data of dimension  $m$ , that is,  $\sigma_0 = \gamma_0$  the baseline pixel-wise bandwidth in the previous clean data experiment.

This falls under the scenario in Section 4.2: As was pointed in the experiment with clean data, normalized clean image  $I_i/\sqrt{m}$  lie on an  $O(1)$  manifold, where  $I_i$  has size  $W \times W$ ,  $m = W^2$ , and thus the pixel-wise bandwidth corresponds to the “ $\gamma$ ” in the theory. If we add Gaussian noise  $\mathcal{N}(0, \sigma_0^2 I_m)$  to the clean image  $I_i$ , it corresponds to adding noise  $\mathcal{N}(0, (\sigma_0^2/m) I_m)$  to  $I_i/\sqrt{m}$ . Thus  $\sigma_0/\sqrt{m}$  is the “ $\sigma$ ” in Section 4.2. The small noise regime in Section 4.2 requires “ $\sigma < c\gamma/\sqrt{m}$ ” for some constant  $c$ , and here, “ $\gamma$ ” there is  $\gamma_0$ , and “ $\sigma$ ” there is  $\sigma_0/\sqrt{m}$ , thus the condition translates into  $\sigma_0/\sqrt{m} < c\gamma_0/\sqrt{m}$ , which is satisfied if we set  $\sigma_0 = \gamma_0$ .



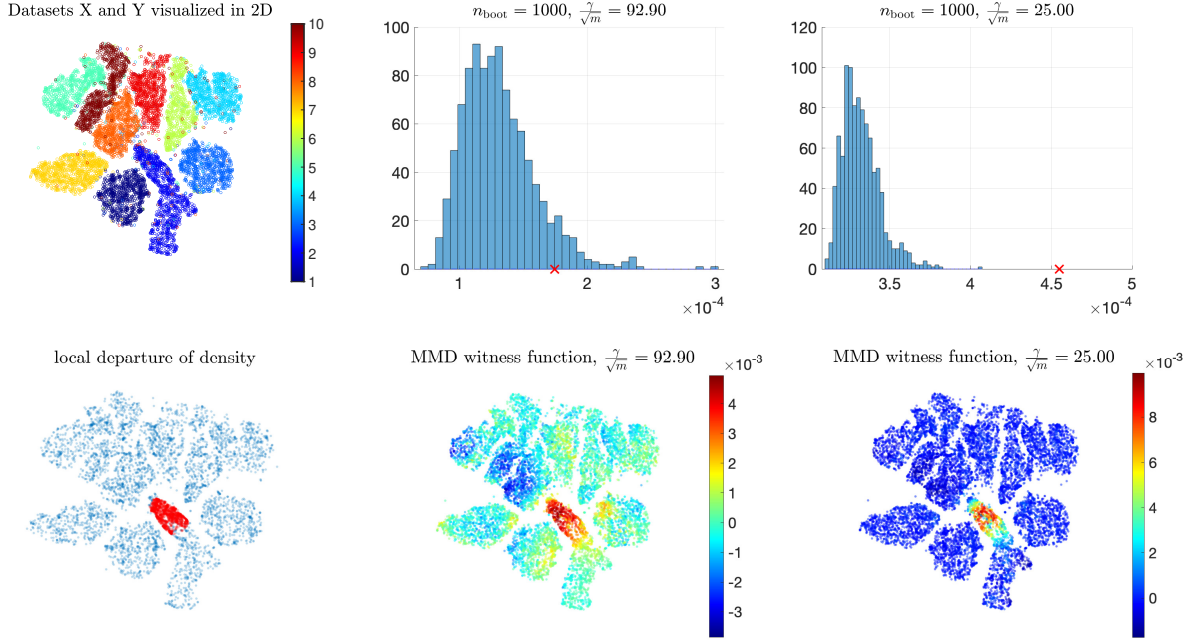


**Figure 3:** MMD two-sample test to detect a local density departure of the MNIST image data distributions. (Top left) Dataset  $X$  and  $Y$  visualized in 2D by tSNE, colored by 10 digit class labels. (Top middle and right) Kernel MMD statistic  $\hat{T}$  (red cross) plotted against the histogram of permutation test, the latter giving an empirical approximation of the distribution of  $\hat{T}|\mathcal{H}_0$ . The middle plot is for kernel MMD using median distance  $\gamma$ , and right plot is by using a smaller  $\gamma$ . (Bottom left) The local cohort density  $p_{\text{cohort}}$  illustrated by red dots. (Bottom middle and right) MMD witness function defined in (23) for kernel using median distance  $\gamma$  and a smaller bandwidth respectively.

An example pair of clean and noise-corrupted images are shown in Figure 2 (Right). We conduct the two-sample testing experiments in the same way as in the experiment with clean data, and the estimated testing power is shown in Figure 2 (Middle). The performance with the four pixel-wise bandwidth which is greater than  $\gamma_0/2$  are about the same as on the clean data; With the smallest pixel bandwidth  $\gamma_0/4$ , the test power degenerates and becomes worse than the choice by median distance, and the drop is more significant when dimensionality  $m$  is small. This suggests that this kernel bandwidth is too small for the amount of additive noise at the values of  $m$  and sample size  $n_X$  and  $n_Y$ .

### 5.3 Density departure on MNIST data

In this experiment, we compute kernel MMD test on the original MNIST digit image dataset, where samples are of dimensionality  $28 \times 28$ . The data densities  $p$  and  $q$  are generated in the following way:  $p$  is uniformly subsample from the MNIST dataset, namely  $p = p_{\text{data}}$ . Though we only have finite samples (the MNIST dataset has 70000 images in 10 classes) of  $p_{\text{data}}$ , as we subsample  $n_X = 6000$  from the whole dataset, it is approximate as if drawn from the population

density.  $q$  is constructed as a mixture of

$$q = 0.975p_{\text{data}} + 0.025p_{\text{cohort}},$$

where  $p_{\text{cohort}}$  is the distribution of a local cohort within the samples of digit ‘1’, having about 1700 samples. Since  $n_Y$  is set to be about 6000, and we subsample about 150 from the local cohort, thus it is approximately drawn from the density of  $p_{\text{cohort}}$ . The local departure of density is illustrated in Figure 3 (Bottom left). The experiment are conducted on one realization of dataset  $X$  and  $Y$ , where  $n_X = 6000$ ,  $n_Y = 5990$ .

We apply kernel MMD test with two bandwidth, one using the median distance, which gives the pixel-wise bandwidth  $\gamma/\sqrt{m} = 92.9$ , and here  $m = 28^2$ ; and the other takes  $\gamma/\sqrt{m} = 25$ . The MMD test statistic  $\hat{T}$  under  $H_1$  vs. the histogram under  $H_0$  computed by permutation test with  $n_{\text{boot}} = 1000$  are shown in the top panel of Figure 3. It can be seen that with the smaller bandwidth, the MMD test statistic shows a more clear rejection of  $H_0$ , indicating better testing power.

The MMD *witness function* [16], defined as

$$\hat{w}(x) = -\frac{1}{n_X} \sum_{i=1}^{n_X} K_{\gamma}(x, x_i) + \frac{1}{n_Y} \sum_{j=1}^{n_Y} K_{\gamma}(x, y_j), \quad (23)$$

is shown as heat-map on the 2D embedding in the bottom panel of Figure 3. The witness function indicates where the two densities differ. Compared with the ground truth in the bottom left plot of the departure  $p_{\text{cohort}}$ , the MMD witness function computed with the local kernel better detects the density departure than the median distance kernel. The better witness function by the local kernel is consistent with the better test statistic separation in the top panel plots.

As a remark, unlike in Subsection 5.2, the MNIST image data do not lie on any constructed manifold induced by latent group action, but only lie near to certain manifold-like structures in the ambient space - the latent manifold reveals all possible variations of images of the 10 digits, and since there are 10 classes, there are possibly 10 sub-manifolds, as illustrated by the 2D embedding by tSNE [43] in Figure 3 (Top left). Thus, the case does not fall under the exact theoretical assumption of manifold data in Section 3, though manifold-like structures are likely to present in the dataset. The experimental results show that a more localized kernel that has a smaller bandwidth than the median distance bandwidth can have better testing power when applied to general manifold-like high-dimensional data.

## 6 Discussion

The work can be extended in several directions. First, we only consider isotropic kernel with fixed bandwidth, and it would be of interest to generalize to other types of kernel used in practice, such as anisotropic kernel using local Mahalanobis distance and other non-Euclidean metrics, kernel with adaptive bandwidth [48, 10], asymmetric kernel  $a(r, x)$  with a reference set  $r \in R$  [25, 9], and so on. Algorithm-wise, it would be desirable to develop efficient kernel testing methods

which can reduce the storage and computational load, e.g., by leveraging neural network tools. Next, it is natural to extend to other kernel-based testing problems, e.g., goodness-of-fit tests [11, 24, 39], and general hypothesis tests. The reduction of sampling complexity by intrinsic low-dimensionality of manifold data may also benefit other kernel-based testing methods. At last, a more systematic study is to be developed for near-manifold data in high-dimensional space. Further, high-dimensional data exhibit more complicated low-dimensional structures than the manifold data assumption, and one can pursue a more general framework to capture the intrinsic low dimensionality, or low complexity, in the data distributions for testing problems.

## 7 Proofs

### 7.1 Proofs in Section 3

*Proof of Lemma 3.1.* We denote by  $B_r^l(x)$  the Euclidean ball in  $\mathbb{R}^l$  of radius  $r > 0$  centered at  $x$ . When  $l = m$ , we omit the superscript  $l$  and use  $B_r(x)$  to denote the Euclidean ball in the ambient space  $\mathbb{R}^m$ . In big-O notation, we use subscript  $_{MC}$  to emphasize constant dependence on manifold curvature,  $_{MV}$  for that on manifold volume, and  $_{GM}$  for that on ‘‘Gaussian moments’’ namely the finitely many moments of normal densities in  $\mathbb{R}^d$ .

First, we use the sub-exponential decay of  $h$  to truncate the integral of  $dV(y)$  in (9) on  $\mathcal{M} \cap B_{\delta_\gamma}(x)$  only, where  $\delta_\gamma := \sqrt{1.2 \frac{d+10}{a} \gamma^2 \log \frac{1}{\gamma}}$ , with an  $O(\|f\|_\infty \gamma^{10})$  residual: When  $\|y - x\| \geq \delta_\gamma$ , by Assumption 3.3(C2),  $h(\frac{\|x-y\|^2}{\gamma^2}) \leq e^{-a\delta_\gamma^2/\gamma^2} = \gamma^{d+10}$ , and then

$$\begin{aligned} |\gamma^{-d} \int_{\mathcal{M} \setminus B_{\delta_\gamma}(x)} h(\frac{\|x-y\|^2}{\gamma^2}) f(y) dV(y)| &\leq \gamma^{-d} \int_{\mathcal{M} \setminus B_{\delta_\gamma}(x)} \gamma^{d+10} |f(y)| dV(y) \\ &\leq \|f\|_\infty \text{Vol}(\mathcal{M}) \gamma^{10} = O_{MV}(\|f\|_\infty \gamma^{10}), \quad \forall x \in \mathcal{M}. \end{aligned} \quad (24)$$

Next, we use local expansion of  $f$  and kernel function to compute the integral of  $dV(y)$  on  $B_{\delta_\gamma}(x)$ .

By compactness of  $\mathcal{M}$ , there is  $\gamma_1(\mathcal{M})$  such that when  $\gamma < \gamma_1$  and then  $\delta_\gamma := \sqrt{\frac{d+10}{a} \gamma^2 \log \frac{1}{\gamma}}$  is sufficiently small,  $B_{\delta_\gamma}(x) \cap \mathcal{M}$  is isomorphic to a ball in  $\mathbb{R}^d$ . This  $\gamma_1(\mathcal{M})$  depends on manifold reach.

Then the local chart is well defined, and we use the local projected coordinate on the tangent plane: Let  $\phi_x$  be the projection to  $T_x(\mathcal{M})$ , for each  $y \in \mathcal{M} \cap B_{\delta_\gamma}(x)$ ,  $u = \phi_x(y - x)$ . By that locally the normal coordinate and the projected coordinate  $s$  matches up to the 3rd order (c.f. Lemma 6 and 7 in [13], also see Lemma A.1 in [10])

$$\begin{aligned} d_{\mathcal{M}}(x, y) &= \|u\|(1 + O_{MC}(\|u\|^2)), \quad \|y - x\| = \|u\|(1 + O_{MC}(\|u\|^2)), \\ \left| \det \left( \frac{dy}{du} \right) \right| &= 1 + O_{MC}(\|u\|^2), \end{aligned} \quad (25)$$

where the constants are uniform for all  $x$ , due to compactness of  $\mathcal{M}$ . Thus, there is another

$\gamma_2(\mathcal{M})$  such that when  $\gamma < \gamma_2$ , for any  $x \in \mathcal{M}$ ,

$$\begin{cases} 0.9\|y - x\| \leq 0.9d_{\mathcal{M}}(x, y) \leq \|u\|_{\mathbb{R}^d} \leq \|y - x\| \leq d_{\mathcal{M}}(x, y), \\ \left| \det \left( \frac{dy}{du} \right) \right| \leq 2, \quad \|y - x\|^2 = \|u\|^2 + O_{MC}(\|u\|^4) \end{cases} \quad \forall y \in \mathcal{M} \cap B_{\delta_\gamma}(x). \quad (26)$$

This  $\gamma_2(\mathcal{M})$  depends on manifold curvature, and is small when manifold curvature has large magnitude.

Set  $\gamma_0 = \min\{\gamma_1, \gamma_2\}$ , when  $\gamma < \min\{\gamma_0, 1\}$ , we have (25) and (26), where the big-O notation means that the corresponding term has absolute value bounded by the implied constant times the quantity inside the  $O(\cdot)$ .

We now expand  $f$  locally at  $x$ , and we separate the two cases,  $\beta \leq 1$ , and  $1 < \beta \leq 2$ .

Case 1:  $\beta \leq 1$ .

Let  $y \in B_{\delta_\gamma}(x) \cap \mathcal{M}$ , because  $f$  has Hölder constant  $L_f$ ,  $|f(y) - f(x)| \leq L_f d_{\mathcal{M}}(x, y)^\beta$ . By (26), and that  $0 < \beta \leq 1$ ,  $d_{\mathcal{M}}(x, y)^\beta \leq \frac{\|u\|^\beta}{0.9^\beta} \leq 0.9^{-1}\|u\|^\beta$ . Thus, with absolute constant in big-O,

$$f(y) = f(x) + O(L_f\|u\|^\beta), \quad \forall y \in \mathcal{M} \cap B_{\delta_\gamma}(x). \quad (27)$$

Meanwhile, by (26) and that  $h$  is  $C^1$  on  $(0, \infty)$ ,

$$h\left(\frac{\|x - y\|^2}{\gamma^2}\right) = h\left(\frac{\|u\|^2 + O_{MC}(\|u\|^4)}{\gamma^2}\right) = h\left(\frac{\|u\|^2}{\gamma^2}\right) + h'(\xi(u))O_{MC}\left(\frac{\|u\|^4}{\gamma^2}\right),$$

where  $\xi(u)$  is between  $\frac{\|u\|^2}{\gamma^2}$  and  $\frac{\|x - y\|^2}{\gamma^2}$ . By (26),  $\xi(u) \geq \frac{\|u\|^2}{\gamma^2}$ , and then by Assumption 3.3 (C2),

$$|h'(\xi(u))| \leq a_1 e^{-a \frac{\|u\|^2}{\gamma^2}}. \quad (28)$$

Then, we define  $B'_x := \phi_x(\mathcal{M} \cap B_{\delta_\gamma}(x)) \subset \mathbb{R}^d$  and have that

$$\gamma^{-d} \int_{\mathcal{M} \cap B_{\delta_\gamma}(x)} h\left(\frac{\|x - y\|^2}{\gamma^2}\right) f(y) dV(y) \quad (29)$$

$$\begin{aligned} &= \gamma^{-d} \int_{B'_x} \left( h\left(\frac{\|u\|^2}{\gamma^2}\right) + a_1 e^{-a \frac{\|u\|^2}{\gamma^2}} O_{MC}\left(\frac{\|u\|^4}{\gamma^2}\right) \right) f(y(u)) \left| \det \left( \frac{dy}{du} \right) \right| du \\ &= \gamma^{-d} \int_{B'_x} h\left(\frac{\|u\|^2}{\gamma^2}\right) (f(x) + O(L_f\|u\|^\beta)) \left| \det \left( \frac{dy}{du} \right) \right| du \\ &\quad + \gamma^{-d} \int_{B'_x} a_1 e^{-a \frac{\|u\|^2}{\gamma^2}} O_{MC}\left(\frac{\|u\|^4}{\gamma^2}\right) \|f\|_\infty \left| \det \left( \frac{dy}{du} \right) \right| du = \textcircled{1} + \textcircled{2} + \textcircled{3}, \end{aligned} \quad (30)$$

where, by (25),

$$\textcircled{1} := f(x)\gamma^{-d} \int_{B'_x} h\left(\frac{\|u\|^2}{\gamma^2}\right)(1 + O_{MC}(\|u\|^2))du,$$

and by (26),  $\left|\det\left(\frac{dy}{du}\right)\right| \leq 2$ ,

$$\textcircled{2} := \gamma^{-d} \int_{B'_x} h\left(\frac{\|u\|^2}{\gamma^2}\right)O(L_f\|u\|^\beta)2du,$$

$$\textcircled{3} := \gamma^{-d} \int_{B'_x} a_1 e^{-a\frac{\|u\|^2}{\gamma^2}} O_{MC}\left(\frac{\|u\|^4}{\gamma^2}\right)\|f\|_\infty 2du.$$

To proceed, note that  $B'_x$  is not a ball on  $\mathbb{R}^d$  but is contained between two spheres: by (26), we have  $B_{0,9\delta_\gamma}^d(0) \subset B'_x \subset B_{\delta_\gamma}^d(0)$ . This together with the exponential decay of  $h$  gives that

$$\begin{aligned} \left| \gamma^{-d} \int_{B'_x} h\left(\frac{\|u\|^2}{\gamma^2}\right)du - m_0 \right| &\leq \left| \gamma^{-d} \int_{\mathbb{R}^d \setminus B_{0,9\delta_\gamma}^d(0)} h\left(\frac{\|u\|^2}{\gamma^2}\right)du \right| \leq \int_{v \in \mathbb{R}^d, \|v\| \geq 0.9\delta_\gamma/\gamma} e^{-a\|v\|^2} dv \\ &= O_{GM,a}(\gamma^{10}). \end{aligned}$$

Meanwhile,  $\gamma^{-d} \int_{B'_x} h\left(\frac{\|u\|^2}{\gamma^2}\right)\|u\|^2 du = O_{GM,a}(\gamma^2)$ . Thus,

$$\textcircled{1} = f(x)(m_0[h] + O_{GM,a}(\gamma^{10}) + O_{GM,a,MC}(\gamma^2)) = m_0 f(x) + O_{GM,a,MC}(\|f\|_\infty \gamma^2).$$

Similarly,  $\gamma^{-d} \int_{B'_x} h\left(\frac{\|u\|^2}{\gamma^2}\right)\|u\|^\beta du = O_{GM,a}(\gamma^\beta)$ , and then

$$\textcircled{2} = O_{GM,a}(L_f \gamma^\beta).$$

Finally,  $\gamma^{-d} \int_{B'_x} a_1 e^{-a\frac{\|u\|^2}{\gamma^2}} \frac{\|u\|^4}{\gamma^2} du = O_{GM,a}(\gamma^2)$ , and then

$$\textcircled{3} = O_{GM,a,MC}(\|f\|_\infty \gamma^2).$$

Putting together, we have that (7.1) equals

$$\textcircled{1} + \textcircled{2} + \textcircled{3} = m_0[h]f(x) + O_{GM,a,MC}(\|f\|_\infty \gamma^2) + O_{GM,a}(L_f \gamma^\beta),$$

and the integral outside  $B_{\delta_\gamma}(x)$  gives  $O_{MV}(\|f\|_\infty \gamma^{10})$  as shown in (24). Because  $\gamma < 1$ ,  $\gamma^{10} \leq \gamma^2$ . Combined together, this proves (9) under case 1 with  $C_1$  being some  $C_1^{(\text{case 1})}$  which depends on  $h$  and  $d$  (GM,  $a$ ) and manifold curvature and volume.

Case 1:  $1 < \beta \leq 2$ .

Recall the definition of Hölder constant  $L_f$  when  $\beta > 1$ , the expansion (27) has the the

following counterpart for any  $y \in \mathcal{M} \cap B_{\delta_\gamma}(x)$ ,

$$\begin{aligned} f(y) &= f(x) + \nabla_{\mathcal{M}} f(x)^T (u + O_{MC}(\|u\|^2) + O(L_f \|u\|^\beta)) \\ &= f(x) + \nabla_{\mathcal{M}} f(x)^T u + O_{MC}(L_f \|u\|^\beta). \end{aligned} \quad (31)$$

Then similarly expanding the kernel  $h(\frac{\|x-y\|^2}{\gamma^2})$  in the integral, we have

$$\gamma^{-d} \int_{\mathcal{M} \cap B_{\delta_\gamma}(x)} h(\frac{\|x-y\|^2}{\gamma^2}) f(y) dV(y) = \textcircled{1} + \textcircled{2} + \textcircled{3},$$

where

$$\textcircled{1} := \gamma^{-d} \int_{B'_x} h(\frac{\|u\|^2}{\gamma^2}) (f(x) + \nabla_{\mathcal{M}} f(x)^T u) (1 + O_{MC}(\|u\|^2)) du,$$

and again, since  $\left| \det \left( \frac{dy}{du} \right) \right| \leq 2$ ,

$$\textcircled{2} := \gamma^{-d} \int_{B'_x} h(\frac{\|u\|^2}{\gamma^2}) O_{MC}(L_f \|u\|^\beta) 2du,$$

$$\textcircled{3} := \gamma^{-d} \int_{B'_x} a_1 e^{-a \frac{\|u\|^2}{\gamma^2}} O_{MC}(\frac{\|u\|^4}{\gamma^2}) \|f\|_\infty 2du.$$

Same as before,  $\textcircled{3} = O_{GM,a,MC}(\|f\|_\infty \gamma^2)$ , and  $\textcircled{2} = O_{GM,a,MC}(L_f \gamma^\beta)$ . Also,  $\textcircled{1} = \textcircled{4} + \textcircled{5}$ , where

$$\textcircled{4} = \gamma^{-d} \int_{B'_x} h(\frac{\|u\|^2}{\gamma^2}) (f(x) + \nabla_{\mathcal{M}} f(x)^T u) du \quad (32)$$

$$= m_0 f(x) + f(x) O_{GM,a}(\gamma^{10}) + 0 + \|\nabla_{\mathcal{M}} f(x)\| O_{GM,a}(\gamma^{10}) \quad (33)$$

$$= m_0 f(x) + O_{GM,a}((\|f\|_\infty + \|\nabla_{\mathcal{M}} f(x)\|) \gamma^{10}), \quad (34)$$

where in the 2nd equality we used that the integral of  $h(\frac{\|u\|^2}{\gamma^2}) u du$  vanishes on  $\mathbb{R}^d$ ,

$$\textcircled{5} = \gamma^{-d} \int_{B'_x} h(\frac{\|u\|^2}{\gamma^2}) (f(x) + \nabla_{\mathcal{M}} f(x)^T u) O_{MC}(\|u\|^2) du \quad (35)$$

$$= O_{MC,GM,a}(\|f\|_\infty \gamma^2) + O_{MC,GM,a}(\|\nabla_{\mathcal{M}} f\|_\infty \gamma^3). \quad (36)$$

Putting together, by that  $\|\nabla_{\mathcal{M}} f\|_\infty \leq L_f$ , we have

$$\textcircled{1} = m_0 [h] f(x) + O_{MC,GM,a}(\|f\|_\infty \gamma^2) + O_{MC,GM,a}(L_f \gamma^3),$$

and thus, since  $\gamma^3 \leq \gamma^\beta$ ,

$$\textcircled{1} + \textcircled{2} + \textcircled{3} = m_0 [h] f(x) + O_{GM,a,MC}(L_f \gamma^\beta) + O_{GM,a,MC}(\|f\|_\infty \gamma^2).$$

The integral outside  $B_{\delta_\gamma}(x)$  again can be incorporated into the residual term above because  $\gamma^{10} \leq \gamma^2$ . This proves (9) under case 2 with  $C_1$  being some  $C_1^{(\text{case 2})}$  which depends on  $h$  and  $d$  (GM,  $a$ ) and manifold curvature and volume.

Choosing  $C_1 = \max\{C_1^{(\text{case 1})}, C_1^{(\text{case 2})}\}$  makes (9) hold for both cases.  $\square$

*Proof of Lemma 3.2.* By Lemma 3.1, we have that when  $\gamma < \min\{\gamma_0, 1\}$ ,

$$\mathbb{E}_{x \sim p, y \sim p} K_\gamma(x, y) = \int_{\mathcal{M}} p(x) \left( \int_{\mathcal{M}} K_\gamma(x, y) p(y) dV(y) \right) dV(x) \quad (37)$$

$$= \int_{\mathcal{M}} p(x) \gamma^d (m_0 p(x) + r_1(x)) dV(x), \quad \|r_1\|_\infty \leq C_1 (L_\rho \gamma^\beta + \rho_{\max} \gamma^2) \quad (38)$$

$$= \gamma^d \left( m_0 [h] \int_{\mathcal{M}} p^2 + s_1 \right), \quad |s_1| \leq C_1 (L_\rho \gamma^\beta + \rho_{\max} \gamma^2), \quad (39)$$

where we use the short-handed notation  $\int_{\mathcal{M}} p^2 = \int_{\mathcal{M}} p(x)^2 dV(x)$ . Similarly,

$$\mathbb{E}_{x \sim q, y \sim q} K_\gamma(x, y) = \gamma^d \left( m_0 [h] \int_{\mathcal{M}} q^2 + s_2 \right), \quad (40)$$

$$\mathbb{E}_{x \sim p, y \sim q} K_\gamma(x, y) = \gamma^d \left( m_0 [h] \int_{\mathcal{M}} pq + s_3 \right), \quad (41)$$

$$|s_2|, |s_3| \leq C_1 (L_\rho \gamma^\beta + \rho_{\max} \gamma^2), \quad (42)$$

Thus, by definition of  $T$ ,

$$T = \gamma^d \left( m_0 [h] \int_{\mathcal{M}} (p - q)^2 + s_1 + s_2 - 2s_3 \right),$$

which proves (11) by the bounds of  $|s_1|, |s_2|, |s_3|$ .  $\square$

*Proof of Prop. 3.4.* By definition,

$$\widehat{T} = \widehat{T}_{XX} + \widehat{T}_{YY} - 2\widehat{T}_{XY},$$

where

$$\widehat{T}_{XX} = \frac{1}{n_X^2} \sum_{i, i'=1} K_\gamma(x_i, x_{i'}), \quad \widehat{T}_{YY} = \frac{1}{n_Y^2} \sum_{j, j'=1} K_\gamma(y_j, y_{j'}), \quad \widehat{T}_{XY} = \frac{1}{n_X n_Y} \sum_{i, j} K_\gamma(x_i, y_j),$$

and we analyze the concentration of the three terms respectively. By (2),

$$n_X - 1 \geq 0.9 \rho_X n, \quad n_Y - 1 \geq 0.9 (1 - \rho_X) n,$$

and thus by definition of  $c$  as in (12),

$$cn \leq n_X - 1, n_Y - 1 \leq n. \quad (43)$$

We first analyze  $\widehat{T}_{XX}$ , Since  $K_\gamma(x, x) = h(0) = 1$ ,

$$\widehat{T}_{XX} = \frac{1}{n_X} + (1 - \frac{1}{n_X})V_{XX}, \quad V_{XX} := \frac{1}{n_X(n_X - 1)} \sum_{i \neq j, i, j=1}^{n_X} K_\gamma(x_i, x_j).$$

We write  $n_X = N$  for a short-handed notation. Define, for  $i \neq j$ ,  $V_{i,j} := K_\gamma(x_i, x_j)$ , we have that

$$\mathbb{E}V_{i,j} = \mathbb{E}_{x \sim p, y \sim p} K_\gamma(x, y).$$

Meanwhile, by that  $|h| \leq 1 := L_V$  as in Assumption 3.3 (C2), we always have  $|V_{ij}| \leq 1$ . The variance

$$\text{Var}(V_{ij}) \leq \mathbb{E}V_{ij}^2 = \int_{\mathcal{M}} \int_{\mathcal{M}} h^2 \left( \frac{\|x - y\|^2}{\gamma^2} \right) p(x)p(y) dV(x) dV(y).$$

Note that  $h_2 := h^2$  also satisfies Assumption 3.3 (with constants  $a$  replaced  $2a$ , same  $a_0 = 1$  and  $a_1$  replaced by  $2a_1$ ), and thus one can apply Lemma 3.1 with  $h$  replace by  $h_2$ , which does not change the threshold constant  $\gamma_0$ , but the constant  $C_1$  in the error bound changes to  $C_1^{(2)}$  corresponding to the new kernel function  $h_2$ . Since  $\gamma < \min\{1, \gamma_0\}$ , applying Lemma 3.1 with  $h_2$  and  $f = 1$  gives that

$$\left| \gamma^{-d} \int_{\mathcal{M}} h^2 \left( \frac{\|x - y\|^2}{\gamma^2} \right) dV(y) - m_0[h^2] \right| \leq C_1^{(2)} \gamma^2.$$

Thus

$$\begin{aligned} \mathbb{E}V_{ij}^2 &\leq \gamma^d \|p\|_\infty \int_{\mathcal{M}} p(x) \left( m_0[h^2] + C_1^{(2)} \gamma^2 \right) dV(x) \\ &\leq \gamma^d \rho_{\max} \left( m_0[h^2] + C_1^{(2)} \gamma^2 \right), \end{aligned} \quad (44)$$

Since we assume  $\gamma < \frac{1}{\sqrt{C_1^{(2)}}}$  in the condition, by definition of  $\nu$  as in (12), we then have that

$$\text{Var}(V_{ij}) \leq \gamma^d \nu. \quad (45)$$

We use the decoupling of U-statistics: Define  $\tilde{V}_{i,j} = V_{i,j} - \mathbb{E}V_{i,j}$  for  $i \neq j$ . For any  $s > 0$ , let



$\mathcal{S}_N$  be denote the permutation group of  $N$  elements, we have

$$\begin{aligned} V_{XX} &= \frac{1}{N(N-1)} \sum_{i \neq j} \tilde{V}_{i,j} = \frac{1}{N!} \frac{1}{N(N-1)} \sum_{\gamma \in \mathcal{S}_N} \sum_{i \neq j} \tilde{V}_{\gamma(i), \gamma(j)} \\ &= \frac{1}{N!} \frac{1}{\lfloor N/2 \rfloor} \sum_{\gamma \in \mathcal{S}_N} \sum_{i=1}^{\lfloor N/2 \rfloor} \tilde{V}_{\gamma(2i-1), \gamma(2i)}. \end{aligned}$$

Then, by Jensen's inequality, let  $M = \lfloor N/2 \rfloor$ ,

$$\mathbb{E} e^{sV_{XX}} \leq \frac{1}{N!} \sum_{\gamma \in \mathcal{S}_N} \mathbb{E} \exp\left\{s \frac{1}{M} \sum_{i=1}^M \tilde{V}_{\gamma(2i-1), \gamma(2i)}\right\} = \mathbb{E} \exp\left\{s \frac{1}{M} \sum_{i=1}^M \tilde{V}_{2i-1, 2i}\right\},$$

and the sum over  $i$  is an independent sum over  $M$  random variables. By that  $|\tilde{V}_{ij}| \leq 1$ , and (45), then same as in the derivation of the classical Bernstein's inequality, we have that for any  $t > 0$ ,

$$\mathbb{P}[V_{XX} - \mathbb{E}V_{ij} > t] \leq \exp\left\{-\frac{\lfloor N/2 \rfloor t^2}{2\gamma^d \nu + \frac{2}{3}tL_V}\right\} \leq \exp\left\{-\frac{(N-1)t^2}{2(2\gamma^d \nu + \frac{2}{3}tL_V)}\right\}.$$

We target at

$$t = \lambda \sqrt{\frac{\gamma^d \nu}{N-1}}, \quad \lambda > 0,$$

and when

$$\frac{tL_V}{3} < \gamma^d \nu, \tag{46}$$

the tail probability is bounded by

$$\exp\left\{-\frac{(N-1)t^2}{8\gamma^d \nu}\right\} = \exp\left\{-\frac{\lambda^2}{8}\right\}.$$

By that  $L_V = 1$ , (46) is equivalent to  $\lambda \sqrt{\frac{\gamma^d \nu}{N-1}} < 3\gamma^d \nu$  which is

$$0 < \lambda < 3\sqrt{\nu\gamma^d(N-1)}.$$

This proves that

$$\mathbb{P}[V_{XX} - \mathbb{E}V_{ij} > \lambda \sqrt{\frac{\gamma^d \nu}{(N-1)}}] \leq e^{-\lambda^2/8}, \quad \forall 0 < \lambda < 3\sqrt{\nu\gamma^d(N-1)}. \tag{47}$$

The low-tail can be proved similarly, so we have

$$\mathbb{P} \left[ V_{XX} - \mathbb{E}_{x \sim p, y \sim p} K_\gamma(x, y) > \lambda \sqrt{\frac{\gamma^d \nu}{n_X - 1}} \right] \leq e^{-\lambda^2/8}, \quad \forall 0 < \lambda < 3\sqrt{\nu \gamma^d (n_X - 1)}, \quad (48)$$

and same for  $\mathbb{P}[V_{XX} - \mathbb{E}_{x \sim p, y \sim p} K_\gamma(x, y) < -\lambda \sqrt{\frac{\gamma^d \nu}{n_X - 1}}]$ .

Similarly, we have

$$\widehat{T}_{YY} = \frac{1}{n_Y} + (1 - \frac{1}{n_Y})V_{YY}, \quad V_{YY} := \frac{1}{n_Y(n_Y - 1)} \sum_{i \neq j, i, j=1}^{n_Y} K_\gamma(y_i, y_j).$$

and

$$\mathbb{P} \left[ V_{YY} - \mathbb{E}_{x \sim q, y \sim q} K_\gamma(x, y) > \lambda \sqrt{\frac{\gamma^d \nu}{n_Y - 1}} \right] \leq e^{-\lambda^2/8}, \quad \forall 0 < \lambda < 3\sqrt{\nu \gamma^d (n_Y - 1)}, \quad (49)$$

and same for  $\mathbb{P} \left[ V_{YY} - \mathbb{E}_{x \sim q, y \sim q} K_\gamma(x, y) < -\lambda \sqrt{\frac{\gamma^d \nu}{n_Y - 1}} \right]$ .

To analyze  $\widehat{T}_{XY}$ , define  $M := \min\{n_X, n_Y\}$ , and

$$\tilde{V}_{i,j} = K_\gamma(x_i, y_j) - \mathbb{E}_{x \sim p, y \sim q} K_\gamma(x, y), \quad i = 1, \dots, n_X, y = 1, \dots, n_Y.$$

Then for any  $s > 0$ , let  $\mathcal{S}_X$  and  $\mathcal{S}_Y$  denote the permutation group of  $n_X$  and  $n_Y$  elements respectively, we then have

$$\begin{aligned} \frac{1}{n_X n_Y} \sum_{i=1}^{n_X} \sum_{j=1}^{n_Y} \tilde{V}_{i,j} &= \frac{1}{n_X!} \frac{1}{n_Y!} \frac{1}{n_X n_Y} \sum_{\gamma_X \in \mathcal{S}_X} \sum_{\gamma_Y \in \mathcal{S}_Y} \sum_{i=1}^{n_X} \sum_{j=1}^{n_Y} \tilde{V}_{\gamma_X(i), \gamma_Y(j)} \\ &= \frac{1}{n_X!} \frac{1}{n_Y!} \frac{1}{M} \sum_{\gamma_X \in \mathcal{S}_X} \sum_{\gamma_Y \in \mathcal{S}_Y} \sum_{i=1}^M \tilde{V}_{\gamma_X(i), \gamma_Y(i)}. \end{aligned}$$

Then, by Jensen's inequality,

$$\begin{aligned} \mathbb{E} \exp \left\{ s \frac{1}{n_X n_Y} \sum_{i=1}^{n_X} \sum_{j=1}^{n_Y} \tilde{V}_{i,j} \right\} &\leq \frac{1}{n_X!} \frac{1}{n_Y!} \sum_{\gamma_X \in \mathcal{S}_X} \sum_{\gamma_Y \in \mathcal{S}_Y} \mathbb{E} \exp \left\{ s \frac{1}{M} \sum_{i=1}^M \tilde{V}_{\gamma_X(i), \gamma_Y(i)} \right\} \\ &= \mathbb{E} \exp \left\{ s \frac{1}{M} \sum_{i=1}^M \tilde{V}_{i,i} \right\}, \end{aligned}$$

and  $\tilde{V}_{i,i} = K_\gamma(x_i, y_i) - \mathbb{E} K_\gamma(x_i, y_i)$  across  $i = 1, \dots, M$  are independent. By that  $|\tilde{V}_{ij}| \leq 1$ , and

same as before, by applying Lemma 3.1 with  $h^2$  and use that  $\gamma < \frac{1}{\sqrt{C_1^{(2)}}}$ ,

$$\text{Var}(\tilde{V}_{ij}) \leq \mathbb{E}V_{ij}^2 = \int_{\mathcal{M}} \int_{\mathcal{M}} h^2 \left( \frac{\|x - y\|^2}{\gamma^2} \right) p(x)q(y) dV(x) dV(y) \leq \gamma^d \nu,$$

then same as in proving (47), we have

$$\mathbb{P} \left[ \hat{T}_{XY} - \mathbb{E}_{x \sim p, y \sim q} K_\gamma(x, y) > \lambda \sqrt{\frac{\gamma^d \nu}{M}} \right] \leq e^{-\lambda^2/8}, \quad \forall 0 < \lambda < 3\sqrt{\nu \gamma^d M}, \quad (50)$$

and same for  $\mathbb{P} \left[ \hat{T}_{XY} - \mathbb{E}_{x \sim p, y \sim q} K_\gamma(x, y) < -\lambda \sqrt{\frac{\gamma^d \nu}{M}} \right]$ .

Recall that

$$\hat{T} = (V_{XX} + V_{YY} - 2\hat{T}_{XY}) + \frac{1}{n_X}(1 - V_{XX}) + \frac{1}{n_Y}(1 - V_{YY}),$$

we now collect (48), (49), (50) to derive concentration of  $\hat{T}$  under  $H_0$  and  $H_1$  respectively:

Under  $H_0$ , we consider upperbound of  $\hat{T}$ . By that  $|V_{XX}|, |V_{YY}| \leq 1$ ,

$$\hat{T} \leq (V_{XX} + V_{YY} - 2\hat{T}_{XY}) + 2\left(\frac{1}{n_X} + \frac{1}{n_Y}\right),$$

and thus, by that  $n_X - 1, n_Y - 1 \geq cn$ , for any  $\lambda < 3\sqrt{c\nu\gamma^d n}$ , w.p.  $> 1 - 3e^{-\lambda^2/8}$ ,

$$\hat{T} \leq \frac{4}{cn} + 4\lambda \sqrt{\frac{\gamma^d \nu}{cn}},$$

because  $(\mathbb{E}_{x \sim p, y \sim p} + \mathbb{E}_{x \sim q, y \sim q} - 2\mathbb{E}_{x \sim p, y \sim q})K_\gamma(x, y) = 0$  when  $p = q$ .

Under  $H_1$ , because  $1 - V_{XX}, 1 - V_{YY} \geq 0$ ,

$$\hat{T} \geq V_{XX} + V_{YY} - 2\hat{T}_{XY}.$$

By the definition of  $T$  and the concentration of  $V_{XX}$ ,  $V_{YY}$ , and  $\hat{T}_{XY}$  as above, using  $n_X, n_Y \geq cn$  again, we have that for any  $\lambda < 3\sqrt{c\nu\gamma^d n}$ , w.p.  $\geq 1 - 3e^{-\lambda^2/8}$ ,

$$\hat{T} \geq T - 4\lambda \sqrt{\frac{\gamma^d \nu}{cn}}.$$

□

## 7.2 Proofs in Subsection 4.1

*Proof of Lemma 4.1.* The proof uses same technique as Lemma 3.1 and the handling of  $x$  near boundary follows the method of Lemma 9 in [13].

The constant  $\gamma'_0$  is defined similarly as before, to guarantee the existence of local chart at

point  $x$  both away from and near boundary (including the uniqueness of the Euclidean distance nearest point  $x_0 \in \partial\mathcal{M}$  to each  $x$  when  $d_E(x, \partial\mathcal{M}) \leq \delta_\gamma$ ), along with the local metric and volume comparison after using projected coordinates  $u$  as (25) and (26). The existence of such  $\gamma'_0$  is due to compactness of  $\mathcal{M}$ . By truncating the integral of  $dV(y)$  on  $B_{\delta_\gamma}(x) \cap \mathcal{M}$  same as before, when  $d_E(x, \partial\mathcal{M}) > \delta_\gamma$ , the claim follows the proof of Lemma 3.1 with the constant  $C_1$  be some  $C'_{1,interior}$ .

To analyze the case for  $x$  where  $d_E(x, \partial\mathcal{M}) \leq \delta_\gamma$ , let  $x_0 \in \partial\mathcal{M}$  be the nearest point on the boundary to  $x$  under Euclidean distance, and we follow the same change of coordinates around  $x_0$  as in the proof of Lemma 9 in [13]. By the symmetry of the kernel  $h(\frac{\|u\|^2}{\gamma^2})$  and the same analysis in Lemma 9 of [13], one can show that

$$\gamma^{-d} \int_{B_{\delta_\gamma}(x) \cap \mathcal{M}} h\left(\frac{\|x-y\|^2}{\gamma^2}\right) f(y) dV(y) = f(x) m_0^{(\gamma)}[h](x) + O_{GM,a}(L_f \gamma^\beta) + O_{GM,a,MC}(\|f\|_\infty \gamma^2)$$

where  $m_0^{(\gamma)}[h](x)$  equals the integral of  $\gamma^{-d} h(\frac{\|u\|^2}{\gamma^2})$  on a partial domain in  $\mathbb{R}^d$  and the domain depends on the location of  $x$ , defined in the same way as in Lemma 9 in [13] and satisfies  $m_0^{(\gamma)}[h](x) \leq m_0[h]$ ; The  $O_{GM,a}(L_f \gamma^\beta)$  term is due to the expansion of  $f$  near  $x$ , and the  $O_{GM,a,MC}(\|f\|_\infty \gamma^2)$  due to the expansion of kernel and the volume form  $|\det(\frac{dy}{du})| = 1 + O(\|u\|^2)$ , similar as in the proof of Lemma 3.1. Putting together, this proves (19) with the bound  $C'_{1,boundary}(L_f \gamma^\beta + \|f\|_\infty \gamma^2)$  on the r.h.s.

Taking  $C' = \max\{C'_{1,interior}, C'_{1,boundary}\}$  finishes the proof of the lemma.  $\square$

*Proof of Lemma 4.2.* By Lemma 4.1, when  $\gamma < \min\{\gamma_0, 1\}$ , define  $P_\gamma := \{x \in \mathcal{M}, d_E(x, \partial\mathcal{M}) \leq \delta_\gamma\}$  which is the near-boundary set,

$$\begin{aligned} \mathbb{E}_{x \sim p, y \sim p} K_\gamma(x, y) &= \int_{\mathcal{M}} p(x) \left( \int_{\mathcal{M}} K_\gamma(x, y) p(y) dV(y) \right) dV(x) \\ &= \int_{\mathcal{M} \setminus P_\gamma} p(x) \gamma^d (m_0[h] p(x) + r_1(x)) dV(x) + \int_{P_\gamma} p(x) \gamma^d (m_0^{(\gamma)}[h](x) p(x) + r_1(x)) dV(x) \\ &= \gamma^d \left( \int_{\mathcal{M} \setminus P_\gamma} m_0[h] p(x)^2 dV(x) + \int_{P_\gamma} m_0^{(\gamma)}[h](x) p(x)^2 dV(x) + \int_{\mathcal{M}} p(x) r_1(x) dV(x) \right), \end{aligned} \quad (51)$$

where

$$\|r_1\|_\infty \leq C'_1(L_\rho \gamma^\beta + \rho_{\max} \gamma^2).$$

Note that

$$\begin{aligned}
& \left| m_0[h] \int_{\mathcal{M} \setminus P_\gamma} p^2 + \int_{P_\gamma} m_0^{(\gamma)}[h](x) p(x)^2 dV(x) - m_0[h] \int_{\mathcal{M}} p^2 \right| \\
&= \left| \int_{P_\gamma} (m_0^{(\gamma)}[h](x) - m_0[h]) p(x)^2 dV(x) \right| \leq \int_{P_\gamma} |m_0^{(\gamma)}[h](x) - m_0[h]| p(x)^2 dV(x) \\
&\leq m_0[h] \int_{P_\gamma} p(x)^2 dV(x) \quad (\text{by that } 0 \leq m_0^{(\gamma)}[h](x) \leq m_0[h] \text{ for all } x) \\
&\leq m_0[h] \rho_{\max}^2 \int_{P_\gamma} dV(x),
\end{aligned}$$

where the volume of the domain  $P_\gamma$  can be shown to be upper bounded by

$$\int_{P_\gamma} dV(x) \leq c_2 \delta_\gamma |\partial \mathcal{M}|,$$

for some constant  $c_2$  depending on the curvature of  $\mathcal{M}$  and the regularity of  $\partial \mathcal{M}$ . Back to (51), this gives that

$$\mathbb{E}_{x \sim p, y \sim p} K_\gamma(x, y) = \gamma^d \left( m_0[h] \int_{\mathcal{M}} p^2 + s'_1 + s_1 \right),$$

where

$$|s'_1| \leq m_0[h] c_2 |\partial \mathcal{M}| \cdot \rho_{\max}^2 \delta_\gamma, \quad |s_1| \leq C'_1 (L_\rho \gamma^\beta + \rho_{\max} \gamma^2).$$

The computation of  $\mathbb{E}_{x \sim q, y \sim q} K_\gamma(x, y)$  and  $\mathbb{E}_{x \sim p, y \sim q} K_\gamma(x, y)$  are similar. Putting together as in the proof of Lemma 3.2, this proves (20) by the definition of  $\delta_\gamma$ , with the constant  $C'_2$  as stated.  $\square$

- Proof of (21) when  $\gamma < \frac{1}{\sqrt{C'_1(2)}}$

*Proof.* Similarly as in the proof of Proposition 3.4, by considering  $h_2 = h^2$  as the kernel function,

$$\begin{aligned}
\mathbb{E}_{x \sim p, y \sim p} K_\gamma(x, y)^2 &\leq \int_{\mathcal{M}} p(x) \rho_{\max} \left( \int_{\mathcal{M}} K_\gamma(x, y)^2 dV(y) \right) dV(x) \\
&= \rho_{\max} \gamma^d \left( \int_{\mathcal{M} \setminus P_\gamma} p(x) (m_0[h^2] + r_2(x)) dV(x) + \int_{P_\gamma} p(x) (m_0^{(\gamma)}[h^2](x) + r_2(x)) dV(x) \right) \\
&\leq \rho_{\max} \gamma^d \left( \int_{\mathcal{M}} m_0[h^2] p(x) dV(x) + \int_{\mathcal{M}} p(x) |r_2(x)| dV(x) \right), \quad (\text{by that } m_0^{(\gamma)}[h^2](x) \leq m_0[h^2])
\end{aligned} \tag{52}$$

where, by applying Lemma 4.1 with  $h$  replaced by  $h^2$  and  $f = 1$ , we have that for constant  $C'_1(2)$  which depends on  $(\mathcal{M}, h)$  (corresponding to  $C'_1$  in Lemma 4.1 with the kernel  $h^2$ )

$$\|r_2\|_\infty \leq C_1'^{(2)}\gamma^2.$$

Thus,

$$\mathbb{E}_{x \sim p, y \sim p} K_\gamma(x, y)^2 \leq \gamma^d \rho_{\max} \left( m_0[h^2] + C_1'^{(2)}\gamma^2 \right)$$

which is bounded by  $\gamma^d \nu$  when  $C_1'^{(2)}\gamma^2 < 1$ .  $\square$

### 7.3 Proofs in Subsection 4.2

Recall that with Gaussian additive noise in  $\mathbb{R}^m$ , the law of  $x_i$  and  $y_i$  can be written as

$$x_i = x_i^{(c)} + \xi_i^{(1)}, \quad y_j = y_j^{(c)} + \xi_j^{(2)}, \quad x_i^{(c)} \sim p_{\mathcal{M}}, \quad y_j^{(c)} \sim q_{\mathcal{M}}, \quad \xi_i^{(k)} \sim \mathcal{N}(0, \sigma_{(k)}^2 I_m), \quad k = 1, 2,$$

where  $x_i^{(c)}$ ,  $y_j^{(c)}$ ,  $\xi_i^{(1)}$  and  $\xi_j^{(2)}$  are independent, and  $p_{\mathcal{M}}$  and  $q_{\mathcal{M}}$  are manifold data densities supported on  $\mathcal{M}$  and satisfy Assumption 3.2. We want to show that our theory in Section 3 extends to this case when  $h$  is Gaussian kernel and the noise level  $\sigma := \sqrt{\sigma_{(1)}^2 + \sigma_{(2)}^2} \leq \frac{c}{\sqrt{m}}\gamma$  for some constant  $c$ .

Though  $p$  and  $q$  are now supported on the ambient space, by the form of  $p$  and  $q$  and  $h(\xi) = e^{-\xi^2/2}$ , we have that

$$\begin{aligned} & \int_{\mathbb{R}^m} \int_{\mathbb{R}^m} K_\gamma(x, y) p(x) p(y) dx dy \\ &= \int_{\mathcal{M}} \int_{\mathcal{M}} \mathbb{E}_{\xi, \eta} \exp \left\{ -\frac{\|(x_1 + \xi) - (y_1 + \eta)\|^2}{2\gamma^2} \right\} p_{\mathcal{M}}(x_1) p_{\mathcal{M}}(y_1) dx_1 dy_1 \\ &= \int_{\mathcal{M}} \int_{\mathcal{M}} \mathbb{E}_g \exp \left\{ -\frac{\|(x_1 - y_1)/\gamma + g\|^2}{2} \right\} p_{\mathcal{M}}(x_1) p_{\mathcal{M}}(y_1) dx_1 dy_1, \quad g \sim \mathcal{N}(0, \frac{\sigma^2}{\gamma^2} I_m). \end{aligned}$$

Define  $\tilde{\sigma}^2 := \frac{\sigma^2}{\gamma^2}$ , we have that for any vector  $v \in \mathbb{R}^m$ ,

$$\mathbb{E}_g \exp \left\{ -\frac{\|v + g\|^2}{2} \right\} = \frac{1}{(1 + \tilde{\sigma}^2)^{m/2}} \exp \left\{ -\frac{\|v\|^2}{2(1 + \tilde{\sigma}^2)} \right\},$$

thus  $\int_{\mathbb{R}^m} \int_{\mathbb{R}^m} K_\gamma(x, y) p(x) p(y) dx dy$  can be equivalently written as

$$\int_{\mathcal{M}} \int_{\mathcal{M}} \frac{1}{(1 + \tilde{\sigma}^2)^{m/2}} \exp \left\{ -\frac{\|x_1 - y_1\|^2}{2\gamma^2(1 + \tilde{\sigma}^2)} \right\} p_{\mathcal{M}}(x_1) p_{\mathcal{M}}(y_1) dx_1 dy_1. \quad (53)$$

Because  $h(\xi)^2 = e^{-\xi}$ , the integral of  $K_\gamma(x, y)^2$  can be computed similarly and it gives

$$\begin{aligned}
& \int_{\mathbb{R}^m} \int_{\mathbb{R}^m} K_\gamma(x, y)^2 p(x) p(y) dx dy \\
&= \int_{\mathcal{M}} \int_{\mathcal{M}} \mathbb{E}_{\xi, \eta} \exp \left\{ -\frac{\|(x_1 + \xi) - (y_1 + \eta)\|^2}{\gamma^2} \right\} p_{\mathcal{M}}(x_1) p_{\mathcal{M}}(y_1) dx_1 dy_1 \\
&= \int_{\mathcal{M}} \int_{\mathcal{M}} \frac{1}{(1 + 2\tilde{\sigma}^2)^{m/2}} \exp \left\{ -\frac{\|x_1 - y_1\|^2}{\gamma^2(1 + 2\tilde{\sigma}^2)} \right\} p_{\mathcal{M}}(x_1) p_{\mathcal{M}}(y_1) dx_1 dy_1. \tag{54}
\end{aligned}$$

Since  $\sigma \leq \frac{c}{\sqrt{m}}\gamma$ ,  $\tilde{\sigma}^2 \leq \frac{1}{m}c^2$ , and then  $1 \leq (1 + \tilde{\sigma}^2)^{m/2} \leq (1 + \frac{c^2}{m})^{m/2} \leq \exp\{c^2/2\}$ , which means that the normalizing constant in (53) is bounded to be  $O(1)$  constant. The same holds for that normalizing constant in (54), namely  $1 \leq (1 + 2\tilde{\sigma}^2)^{m/2} \leq \exp\{c^2\}$ . This means that one can apply Lemma 3.1 to compute the integrals in (53) and (54), replacing the  $p$  and  $q$  in the lemma by  $p_{\mathcal{M}}$  and  $q_{\mathcal{M}}$  respectively. We define the new effective kernel bandwidths in the Gaussian kernel:  $\tilde{\gamma}^{(1)} := \gamma\sqrt{1 + \tilde{\sigma}^2}$  for integral of  $K_\gamma(x, y)$  and  $\tilde{\gamma}^{(2)} := \gamma\sqrt{1 + 2\tilde{\sigma}^2}$  for that of  $K_\gamma(x, y)^2$ . Since  $\tilde{\sigma}^2 \leq \frac{1}{m}c^2$ , the ratios of  $\tilde{\gamma}^{(1)}/\gamma$  and  $\tilde{\gamma}^{(2)}/\gamma$  are bounded by absolute constants from above and below. When  $m$  is large, the ratios are bounded to be  $1 + O(m^{-1})$ .

This gives the approximate expression of  $T$  in Lemma 3.2 involving  $D_{p_{\mathcal{M}}, q_{\mathcal{M}}}$ , as well as the boundedness of variance of  $K_\gamma(x_i, x_j)$  (and  $K_\gamma(y_i, y_j)$ ,  $K_\gamma(x_i, y_j)$ ) needed in Proposition 3.4, replacing  $p$  and  $q$  with  $p_{\mathcal{M}}$  and  $q_{\mathcal{M}}$ , and  $\gamma$  with the new effective kernel bandwidths in the analysis. These replacements allows to prove the same result as in Theorem 3.5 (the constants  $L_\rho$  and  $\rho_{\max}$  are with respect to  $p_{\mathcal{M}}$  and  $q_{\mathcal{M}}$ ), where the constants in the bounds need to be adjusted by multiplying some absolute ones.

## References

- [1] Mikhail Belkin and Partha Niyogi. Laplacian eigenmaps for dimensionality reduction and data representation. *Neural computation*, 15(6):1373–1396, 2003.
- [2] Mikhail Belkin and Partha Niyogi. Convergence of laplacian eigenmaps. In *Advances in Neural Information Processing Systems*, pages 129–136, 2007.
- [3] Monowar H Bhuyan, Dhruba Kumar Bhattacharyya, and Jugal K Kalita. Network anomaly detection: methods, systems and tools. *Ieee communications surveys & tutorials*, 16(1):303–336, 2013.
- [4] Mikołaj Bińkowski, Dougal J. Sutherland, Michael Arbel, and Arthur Gretton. Demystifying mmd gans, 2018.
- [5] Karsten M Borgwardt, Arthur Gretton, Malte J Rasch, Hans-Peter Kriegel, Bernhard Schölkopf, and Alex J Smola. Integrating structured biological data by kernel maximum mean discrepancy. *Bioinformatics*, 22(14):e49–e57, 2006.
- [6] Yang Cao, Vincent Guigues, Anatoli Juditsky, Arkadi Nemirovski, and Yao Xie. Change detection via affine and quadratic detectors, 2018.
- [7] Varun Chandola, Arindam Banerjee, and Vipin Kumar. Anomaly detection: A survey. *ACM Comput. Surv.*, 41(3), July 2009.

- [8] Varun Chandola, Arindam Banerjee, and Vipin Kumar. Anomaly detection for discrete sequences: A survey. *IEEE transactions on knowledge and data engineering*, 24(5):823–839, 2010.
- [9] Xiuyuan Cheng, Alexander Cloninger, and Ronald R Coifman. Two-sample statistics based on anisotropic kernels. *Information and Inference: A Journal of the IMA*, 9(3):677–719, 2020.
- [10] Xiuyuan Cheng and Hau-Tieng Wu. Convergence of graph laplacian with knn self-tuned kernels. *arXiv preprint arXiv:2011.01479*, 2020.
- [11] Kacper Chwialkowski, Heiko Strathmann, and Arthur Gretton. A kernel test of goodness of fit. *JMLR: Workshop and Conference Proceedings*, 2016.
- [12] Kacper P Chwialkowski, Aaditya Ramdas, Dino Sejdinovic, and Arthur Gretton. Fast two-sample testing with analytic representations of probability measures. In *Advances in Neural Information Processing Systems*, pages 1981–1989, 2015.
- [13] Ronald R Coifman and Stéphane Lafon. Diffusion maps. *Applied and computational harmonic analysis*, 21(1):5–30, 2006.
- [14] Eustasio del Barrio, Juan A. Cuesta-Albertos, Carlos Matrán, and Jesús M. Rodríguez-Rodríguez. Tests of goodness of fit based on the  $l_2$ -wasserstein distance. *Ann. Statist.*, 27(4):1230–1239, 08 1999.
- [15] Arthur Gretton, Karsten M. Borgwardt, Malte J. Rasch, Bernhard Schölkopf, and Alexander Smola. A kernel two-sample test. *J. Mach. Learn. Res.*, 13:723–773, March 2012.
- [16] Arthur Gretton, Karsten M Borgwardt, Malte J Rasch, Bernhard Schölkopf, and Alexander Smola. A kernel two-sample test. *Journal of Machine Learning Research*, 13(Mar):723–773, 2012.
- [17] Arthur Gretton, Kenji Fukumizu, Zaïd Harchaoui, and Bharath K. Sriperumbudur. A fast, consistent kernel two-sample test. In Y. Bengio, D. Schuurmans, J. D. Lafferty, C. K. I. Williams, and A. Culotta, editors, *Advances in Neural Information Processing Systems 22*, pages 673–681. Curran Associates, Inc., 2009.
- [18] Arthur Gretton, Dino Sejdinovic, Heiko Strathmann, Sivaraman Balakrishnan, Massimiliano Pontil, Kenji Fukumizu, and Bharath K. Sriperumbudur. Optimal kernel choice for large-scale two-sample tests. In F. Pereira, C. J. C. Burges, L. Bottou, and K. Q. Weinberger, editors, *Advances in Neural Information Processing Systems 25*, pages 1205–1213. Curran Associates, Inc., 2012.
- [19] László Györfi and Edward C. Van Der Meulen. *A Consistent Goodness of Fit Test Based on the Total Variation Distance*, pages 631–645. Springer Netherlands, Dordrecht, 1991.
- [20] Matthias Hein, Jean-Yves Audibert, and Ulrike Von Luxburg. From graphs to manifolds—weak and strong pointwise consistency of graph laplacians. In *International Conference on Computational Learning Theory*, pages 470–485. Springer, 2005.
- [21] James J Higgins. Introduction to modern nonparametric statistics. 2003.
- [22] W Hoeffding. Probability inequalities for sums of bounded random variables. *Journal of the American Statistical Association*, 58:301, 1963.
- [23] Harold Hotelling. The generalization of student’s ratio. *Ann. Math. Statist.*, 2(3):360–378, 08 1931.
- [24] Wittawat Jitkrittum, Heishiro Kanagawa, and Bernhard Schölkopf. Testing goodness of fit of conditional density models with kernels. In *Conference on Uncertainty in Artificial Intelligence*, pages 221–230. PMLR, 2020.



- [25] Wittawat Jitkrittum, Zoltán Szabó, Kacper P Chwialkowski, and Arthur Gretton. Interpretable distribution features with maximum testing power. In *Advances in Neural Information Processing Systems*, pages 181–189, 2016.
- [26] Wittawat Jitkrittum, Wenkai Xu, Zoltán Szabó, Kenji Fukumizu, and Arthur Gretton. A linear-time kernel goodness-of-fit test. In *Advances in Neural Information Processing Systems*, pages 262–271, 2017.
- [27] Frank J. Massey Jr. The kolmogorov-smirnov test for goodness of fit. *Journal of the American Statistical Association*, 46(253):68–78, 1951.
- [28] Chun-Liang Li, Wei-Cheng Chang, Yu Cheng, Yiming Yang, and Barnabás Póczos. Mmd gan: Towards deeper understanding of moment matching network. In *Advances in Neural Information Processing Systems*, pages 2203–2213, 2017.
- [29] James R Lloyd and Zoubin Ghahramani. Statistical model criticism using kernel two sample tests. In C. Cortes, N. D. Lawrence, D. D. Lee, M. Sugiyama, and R. Garnett, editors, *Advances in Neural Information Processing Systems 28*, pages 829–837. Curran Associates, Inc., 2015.
- [30] James R Lloyd and Zoubin Ghahramani. Statistical model criticism using kernel two sample tests. In *Advances in Neural Information Processing Systems*, pages 829–837, 2015.
- [31] David Lopez-Paz and Maxime Oquab. Revisiting classifier two-sample tests. *arXiv preprint arXiv:1610.06545*, 2016.
- [32] Arkadas Ozakin and Alexander Gray. Submanifold density estimation. *Advances in Neural Information Processing Systems*, 22:1375–1382, 2009.
- [33] J. Pfanzagl and O. Sheynin. Studies in the history of probability and statistics XLIV A forerunner of the t-distribution. *Biometrika*, 83(4):891–898, 12 1996.
- [34] John W. Pratt and Jean D. Gibbons. *Kolmogorov-Smirnov Two-Sample Tests*, pages 318–344. Springer New York, New York, NY, 1981.
- [35] Aaditya Ramdas, Nicolas Garcia, and Marco Cuturi. On wasserstein two sample testing and related families of nonparametric tests, 2015.
- [36] Aaditya Ramdas, Sashank Jakkam Reddi, Barnabás Póczos, Aarti Singh, and Larry Wasserman. On the decreasing power of kernel and distance based nonparametric hypothesis tests in high dimensions. In *Twenty-Ninth AAAI Conference on Artificial Intelligence*, 2015.
- [37] Sashank J. Reddi, Aaditya Ramdas, Barnabás Póczos, Aarti Singh, and Larry Wasserman. On the decreasing power of kernel and distance based nonparametric hypothesis tests in high dimensions, 2014.
- [38] Robert J Serfling. *Approximation theorems of mathematical statistics*, volume 162. John Wiley & Sons, 2009.
- [39] Alexander Shapiro, Yao Xie, and Rui Zhang. Goodness-of-fit tests on manifolds. *IEEE Transactions on Information Theory*, 67(4):2539–2553, 2021.
- [40] Amit Singer. From graph to manifold laplacian: The convergence rate. *Applied and Computational Harmonic Analysis*, 21(1):128–134, 2006.
- [41] Bharath K Sriperumbudur, Kenji Fukumizu, Arthur Gretton, Bernhard Schölkopf, Gert RG Lanckriet, et al. On the empirical estimation of integral probability metrics. *Electronic Journal of Statistics*, 6:1550–1599, 2012.

- [42] Dougal J Sutherland, Hsiao-Yu Tung, Heiko Strathmann, Soumyajit De, Aaditya Ramdas, Alex Smola, and Arthur Gretton. Generative models and model criticism via optimized maximum mean discrepancy. *arXiv preprint arXiv:1611.04488*, 2016.
- [43] Laurens Van Der Maaten. Accelerating t-sne using tree-based algorithms. *The Journal of Machine Learning Research*, 15(1):3221–3245, 2014.
- [44] Ulrike Von Luxburg, Mikhail Belkin, and Olivier Bousquet. Consistency of spectral clustering. *The Annals of Statistics*, pages 555–586, 2008.
- [45] Larry Wasserman. *All of nonparametric statistics*. Springer Science & Business Media, 2006.
- [46] Liyan Xie and Yao Xie. Sequential change detection by optimal weighted  $\ell_2$  divergence, 2020.
- [47] Yao Xie and David Siegmund. Sequential multi-sensor change-point detection. *The Annals of Statistics*, 41(2):670–692, Apr 2013.
- [48] Lihi Zelnik-Manor and Pietro Perona. Self-tuning spectral clustering. In *Advances in neural information processing systems*, pages 1601–1608, 2005.
- [49] Jun Zhao, Ariel Jaffe, Henry Li, Ofir Lindenbaum, Esen Sefik, Ruaidhri Jackson, Xiuyuan Cheng, Richard Flavell, and Yuval Kluger. Detection of differentially abundant cell subpopulations discriminates biological states in scRNA-seq data. *bioRxiv*, page 711929 (to appear at PNAS), 2020.